Int. J. Solids Structures Vol. 27, No. 2, pp. 227–258, 1991
Printed in Great Britain

0020-7683/91 $3.00 + .00

ON TWO-DIMENSIONAL SELF-CONSISTENT MICROMECHANICAL DAMAGE MODELS FOR BRITTLE SOLIDS

J. W. Ju
Department of Civil Engineering and Operations Research, Princeton University, Princeton, NJ 08544, U.S.A.

(*Received* 7 *July* 1989; *in revised form* 10 *January* 1990)

Abstract—Two-dimensional self-consistent micromechanical damage models are presented for microcrack-weakened brittle solids under "cleavage 1" deformation processes. The proposed framework basically follows the previous work of Horii and Nemat-Nasser (1983, *J. Mech. Phys. Solids* 31(2), 155–171) and Sumarac and Krajcinovic (1987, *Mech. Mater.* 6, 39–52). Thermodynamic basis, microcrack opening displacements and damage-induced inelastic compliances are derived. Microcrack evolutions (growth) are characterized through the use of fracture mechanics stability criteria and microstructural microcrack geometry. Mode I, mode II and mixed mode microcrack growth are considered. Simple and efficient computational algorithms as well as three detailed numerical simulations are also presented to illustrate the potential capability of the proposed micromechanical damage models. In particular, no fitted "material parameters" are needed. Moreover, loading, unloading stress paths and microcracks status changes in opening/closing are trivially accommodated in this work.

1. INTRODUCTION

Micromechanical damage models for microcrack-weakened brittle solids are presented within the context of the self-consistent method and damage mechanics. For simplicity, only two-dimensional problems are considered. Though phenomenological continuum damage models provide a viable constitutive framework for efficient modelling of brittle solids (e.g. concrete, mortar and brittle composite materials), typically they do not offer perceptive descriptions of microstructural microcrack kinetics. Further, use of several fitted "material parameters" in damage evolution equations only renders vague and averaged information on underlying microcracking processes at the microscale (Krajcinovic and Fanella, 1986). Therefore, micromechanical damage theories, which incorporate microstructural and micromechanical information into the damage mechanics framework, are warranted.

For a literature review on continuum damage mechanics, see, e.g. Krajcinovic (1984, 1986), Ortiz (1985), Ju (1989). On the other hand, micromechanical damage theories ("process models") are limited in the current literature. Some valuable examples are Wu (1985), Krajcinovic and Fanella (1986), Sumarac and Krajcinovic (1987, 1989), Fanella and Krajcinovic (1988) and Krajcinovic and Sumarac (1989). In addition, micromechanical "*non-process*" damage models (i.e. no microcrack growth) were proposed, for instance, by Budiansky and O'Connel (1976), Hoenig (1979), Horii and Nemat-Nasser (1983) and Kachanov (1987) for *static stable* microcracks. Some single crack stress and crack opening displacement analyses (boundary-value problems) were proposed by, for instance, Willis (1978), Sneddon and Lowengrub (1969), Hoenig (1978, 1982) and Mura (1982). Moreover, certain valuable *non-process*, strong microcrack interaction analyses (not quite damage constitutive theories) were proposed, e.g. by Horii and Nemat-Nasser (1985a), Chudnovsky *et al.* (1987a, b) and Kachanov (1987).

An outline of this paper is as follows. Two-dimensional microcrack opening displacements, effective overall (secant) compliance moduli and thermodynamic basis are given in Section 2 for initially linear elastic (isotropic or anisotropic) brittle solids within the context of the self-consistent method. It is assumed that distributed microcrack concentration justifies the use of effective continuum medium theory. The microdefects are considered as line microcracks and microcrack interaction is assumed to be weak, or at most, moderate. Thus, effects of strong microcrack interaction and exact locations of

microcrack centers are not accounted for in this paper (see Kachanov, 1987). Localization failure modes are not considered, either. In Section 3, mode I, mode II and mixed mode discrete microcrack kinetic equations are examined based on microstructural microcrack geometry and fracture mechanics stability criteria for brittle "cleavage I" deformation processes (Ashby, 1979; Sumarac and Krajcinovic, 1987). No phenomenological (fitted) "material parameters" are used in kinetic equations of microcrack growth. Further, loading unloading stress paths are permitted, and microcrack status changes from opening to closing (or vice versa) are trivially accommodated. In Section 4, we present efficient computational algorithms for the proposed micromechanical damage models. Mode I, mode II, and mixed mode numerical simulations are also presented in Section 4.

2. BASIC FRAMEWORK OF SELF-CONSISTENT ELASTIC-DAMAGE MODELS

In this section, we present thermodynamic basis of damage mechanics, derive and summarize *symmetric* or *non-symmetric* "displacement transformation matrices" $\mathbf{B}'$ and anisotropic overall (secant) elastic-damage compliance moduli $\bar{\mathbf{S}}$ for brittle materials. The matrix material is assumed to be perfectly linear elastic.

2.1. *Thermodynamic basis*

It has been shown [see, e.g. Simo and Ju (1987), Ju (1989)] that there exists a *one-to-one* correspondence between the fourth-order elastic-damage secant compliance tensor $\bar{\mathbf{S}}$ and the fourth-order anisotropic damage tensor $\bar{\mathbf{D}}$ (signifying volume average microcrack density, sizes, orientations and opening/closing status). Therefore, it is rational to treat the secant compliance $\bar{\mathbf{S}}(\bar{\mathbf{D}})$ itself as the anisotropic damage variable. Within the framework of the homogenization concept for inhomogeneous effective continuum medium, let us define the homogenized (volume-average) complementary free energy function as (see also Krajcinovic and Sumarac, 1989)

$$\chi = \tfrac{1}{2}\bar{\boldsymbol{\sigma}} : \bar{\mathbf{S}}(\bar{\mathbf{D}}) : \bar{\boldsymbol{\sigma}} \tag{1}$$

where $\bar{\boldsymbol{\sigma}}$ is the *volume-average* stress tensor (Hill, 1965). By the Clausius–Duhem inequality for isothermal process, we have (with $\bar{\boldsymbol{\varepsilon}}$ denoting the volume-average strain)

$$\dot{\chi} - \dot{\bar{\boldsymbol{\sigma}}} : \bar{\boldsymbol{\varepsilon}} \geqslant 0 \tag{2}$$

where [according to (1)]

$$\dot{\chi} = \dot{\bar{\boldsymbol{\sigma}}} : \bar{\mathbf{S}} : \bar{\boldsymbol{\sigma}} + \tfrac{1}{2}\bar{\boldsymbol{\sigma}} : \dot{\bar{\mathbf{S}}} : \bar{\boldsymbol{\sigma}}. \tag{3}$$

The standard Coleman's method then leads to the following macroscopic stress–strain law and the damage dissipative inequality:

$$\bar{\boldsymbol{\varepsilon}} = \bar{\mathbf{S}} : \bar{\boldsymbol{\sigma}} \tag{4a}$$

$$\tfrac{1}{2}\bar{\boldsymbol{\sigma}} : \dot{\bar{\mathbf{S}}} : \bar{\boldsymbol{\sigma}} \geqslant 0. \tag{4b}$$

From eqn (4b), it is observed that the evolution $\dot{\bar{\mathbf{S}}}$ plays an essential role in microcrack energy dissipation and evolutions (i.e. "process models"). During a damage *loading* process (in which some microcracks increase their lengths), the total strain tensor $\bar{\boldsymbol{\varepsilon}}$ is amenable to an additive decomposition: $\bar{\boldsymbol{\varepsilon}} = \bar{\boldsymbol{\varepsilon}}^{e} + \bar{\boldsymbol{\varepsilon}}^{d}$, with $\bar{\boldsymbol{\varepsilon}}^{e}$ and $\bar{\boldsymbol{\varepsilon}}^{d}$ denoting the elastic and inelastic (damage-induced) strains, respectively. It is assumed that $\bar{\boldsymbol{\varepsilon}}^{d} \approx \mathbf{0}$ upon complete unloading; that is, the residual strain at zero stress is negligible for brittle materials. The elastic-damage secant compliance tensor is also suitable for an additive decomposition: $\bar{\mathbf{S}} = \mathbf{S}^{o} + \mathbf{S}^{d}$, with $\mathbf{S}^{o}$ and $\mathbf{S}^{d}$ denoting the virgin undamaged elastic compliance and the damage-induced additional compliance, respectively [see, e.g. Mura (1982), Horii and Nemat-Nasser (1983)].

It is emphasized that once a material contains distributed microcracks, the material becomes *inelastic* due to its load-path dependency. There are different stress–strain curves corresponding to different load paths leading to same final stress state. Under some loading/unloading paths within the context of "non-process models", a damaged material may exhibit linear and reversible response within a limited range. However, one should not regard the damaged material as a perfectly elastic one. For example, when damage state $\bar{\mathbf{D}}$ is *fixed* (i.e. no microcracks increase their sizes or change opening/closing status) and no frictional slip occurs, the overall response remains linear and reversible and therefore we have $\bar{\boldsymbol{\varepsilon}} = \bar{C}\bar{\chi}\,\bar{C}\bar{\boldsymbol{\sigma}}$ and $\bar{\mathbf{S}} = \bar{C}^2\bar{\chi}\,\bar{C}\bar{\boldsymbol{\sigma}}^2$ (*symmetric*). Nevertheless, this is not true when damage state is not fixed or when frictional slip is taking place. In addition, the differentiation of (4a) renders elastic-damage *tangent* compliance tensor $\bar{\mathbf{S}}^{\text{tang}}$ under damage loading condition:

$$\bar{\mathbf{S}}^{\text{tang}} \equiv \frac{\partial \bar{\boldsymbol{\varepsilon}}}{\partial \bar{\boldsymbol{\sigma}}} = \bar{\mathbf{S}} + \frac{\partial \bar{\mathbf{S}}}{\partial \bar{\boldsymbol{\sigma}}} : \bar{\boldsymbol{\sigma}}. \tag{5}$$

From (5), it is clear that in general, $\bar{\mathbf{S}}^{\text{tang}} \neq \bar{\mathbf{S}}$.

Assuming moderate microcrack concentration and microcracks being away from the representative volume boundaries, we have $\bar{\boldsymbol{\sigma}} \approx \boldsymbol{\sigma}^r$, where $\boldsymbol{\sigma}^r$ signifies the remotely applied stress field around the representative volume boundaries (Hill, 1965). Therefore, the microcrack-induced inelastic strain may be approximately expressed as (Vakulenko and Kachanov, 1971; Kachanov, 1980; Horii and Nemat-Nasser, 1983)

$$\bar{\boldsymbol{\varepsilon}}^{\text{d}} = \frac{1}{2V}\sum_k \left[\int_S (\mathbf{b}\otimes\mathbf{n} + \mathbf{n}\otimes\mathbf{b})\,\mathrm{d}S\right]^{(k)}, \tag{6}$$

where V is the representative volume, Σ is a summation operator over all active (open or sliding) microcracks, $\mathbf{b}$ denotes the crack opening displacement vector, and $\mathbf{n}$ signifies the normal vector associated with $\mathbf{b}$. For two-dimensional line microcracks, eqn (6) can be rephrased as (with A denoting the surface area of the representative volume):

$$\bar{\boldsymbol{\varepsilon}}^{\text{d}} = \frac{1}{2A}\sum_k \left[\int_l (\mathbf{b}\otimes\mathbf{n} + \mathbf{n}\otimes\mathbf{b})\,\mathrm{d}l\right]^{(k)}. \tag{7}$$

As was pointed out by Krajcinovic (1985), the alternative definition of the damage variable in terms of $\bar{\boldsymbol{\varepsilon}}^{\text{d}}$ in (6) or (7) is thermodynamically incorrect. The reason is obvious as follows. During "mode I" elastic unloading, $\mathbf{b}$ decreases and the damage variable [defined by eqn (6) or (7)] changes its state, thus leading to energy dissipation even under "mode I" elastic unloading. Therefore, although eqn (6) is an acceptable measure of the damage-induced inelastic deformation, it is not a good choice for anisotropic damage variable. The derivation of appropriate "thermodynamic force" conjugate to the "rate of change of the microcrack density" will be given in the next section.

2.2. *Elastic-damage secant compliance*

In a two-dimensional setting (e.g. plane strain), eqn (4a) can be rewritten using Voigt's notation [see eqn (22) in Horii and Nemat-Nasser (1983)]

$$\bar{e}_i = \bar{S}_{ij}\bar{\tau}_j; \quad i,j = 1,2,3, \tag{8}$$

where $\bar{e}_1 = \bar{\varepsilon}_{11}$, $\bar{e}_2 = \bar{\varepsilon}_{22}$, $\bar{e}_3 = 2\bar{\varepsilon}_{12}$, $\bar{\tau}_1 = \bar{\sigma}_{11}$, $\bar{\tau}_2 = \bar{\sigma}_{22}$, $\bar{\tau}_3 = \bar{\sigma}_{12}$, and $\bar{\mathbf{S}}$ is a three by three elastic-damage secant compliance matrix. For *open* microcracks, the secant compliance is in fact the *unloading* compliance. Therefore, the secant compliance $\bar{\mathbf{S}}$ is *symmetric* (though anisotropic) according to Section 2.1. In the case of mode II frictional sliding on *closed* microcrack faces, by contrast, the elastic-damage secant compliance $\bar{\mathbf{S}}$ is *nonsymmetric*

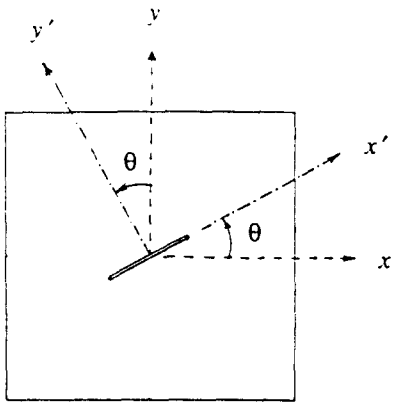

Fig. 1. The local (primed) and global Cartesian coordinate systems.

($\bar{S}'_{ij} \neq \bar{S}'_{ji}$) during either loading or unloading processes. In addition, coordinate transformation matrices $\mathbf{g}$ and $\mathbf{g}'$ relating the secant compliance matrices $\bar{\mathbf{S}}$ and $\bar{\mathbf{S}}'$ (in global and local Cartesian coordinate systems, respectively) are available from eqn (24) in Horii and Nemat-Nasser (1983):

$$\bar{S}'_{ij} = g'_{im}g'_{jn}\bar{S}_{mn}; \quad \bar{S}_{ij} = g_{mi}g_{nj}\bar{S}'_{mn} \tag{9a}$$

$$[\mathbf{g}'] \equiv \begin{bmatrix} \cos^2\theta & \sin^2\theta & \tfrac{1}{2}\sin 2\theta \\ \sin^2\theta & \cos^2\theta & -\tfrac{1}{2}\sin 2\theta \\ -\sin 2\theta & \sin 2\theta & \cos 2\theta \end{bmatrix}; \quad [\mathbf{g}] \equiv \begin{bmatrix} \cos^2\theta & \sin^2\theta & \sin 2\theta \\ \sin^2\theta & \cos^2\theta & -\sin 2\theta \\ -\tfrac{1}{2}\sin 2\theta & \tfrac{1}{2}\sin 2\theta & \cos 2\theta \end{bmatrix}. \tag{9b}$$

It is remarked that the "local" (primed) coordinate system is the intrinsic coordinate system associated with a particular microcrack such that the y'-axis is parallel to the microcrack unit normal vector $\mathbf{n}$, see Fig. 1. Within the context of the self-consistent method, it remains to determine the crack opening displacement $\mathbf{b}'$ across an isolated line-microcrack embedded into an "equivalent" two-dimensional anisotropic homogeneous elastic solid. First, from the geometric compatibility condition, we obtain

$$\frac{\partial^2\bar{e}_1}{\partial y'^2} + \frac{\partial^2\bar{e}_2}{\partial x'^2} - \frac{\partial^2\bar{e}_3}{\partial x'\partial y'} = 0. \tag{10}$$

For an *open* microcrack, substitution of (8) into (10) then yields (Lekhnitskii, 1950)

$$\bar{S}'_{11}\frac{\partial^4 U}{\partial y'^4} - 2\bar{S}'_{13}\frac{\partial^4 U}{\partial x'\partial y'^3} + (2\bar{S}'_{12} + \bar{S}'_{33})\frac{\partial^4 U}{\partial x'^2\partial y'^2} - 2\bar{S}'_{23}\frac{\partial^4 U}{\partial x'^3\partial y'} + \bar{S}'_{22}\frac{\partial^4 U}{\partial x'^4} = 0, \tag{11}$$

where U is a proper stress function. The characteristic equation of (11) takes the form:

$$\bar{S}'_{11}\lambda'^4 - 2\bar{S}'_{13}\lambda'^3 + (2\bar{S}'_{12} + \bar{S}'_{33})\lambda'^2 - 2\bar{S}'_{23}\lambda' + \bar{S}'_{22} = 0. \tag{12}$$

Of course, the elastic-damage secant compliance moduli $\bar{S}'_{ij}$ are as yet *unknown* in accordance with the self-consistent method. According to Lekhnitskii (1950) and Sih *et al.* (1965), the displacement jump across an (kth) *open* microcrack (under mode I or mixed I/II mode) in an anisotropic homogeneous elastic solid can be expressed as:

$$b_1^{(k)} = 2\sqrt{a^{(k)2} - x'^2}\,\bar{S}'_{11}[(r'_1s'_2 + r'_2s'_1)\bar{\tau}'_2 + (s'_1 + s'_2)\bar{\tau}'_3]^{(k)} \tag{13a}$$

$$b_2^{(k)} = 2\sqrt{a^{(k)2} - x'^2}\,\bar{S}'_{22}\left[\left(\frac{s'_1}{r'^2_1 + s'^2_1} + \frac{s'_2}{r'^2_2 + s'^2_2}\right)\bar{\tau}'_2 + \frac{r'_1s'_2 + r'_2s'_1}{[r'^2_1 + s'^2_1][r'^2_2 + s'^2_2]}\bar{\tau}'_3\right]^{(k)}, \tag{13b}$$

where $\lambda_j' = r_j' + is_j'$ ($j = 1, 2$), with $s_1', s_2' > 0$, are the roots of the characteristic equation (12). Equation (12) is a fourth-order equation and can be solved analytically. Further, let us define the two by two "displacement transformation matrix" $\mathbf{B}^{(k)'}$ as:

$$[\mathbf{B}^{(k)'}] \equiv \begin{bmatrix} \bar{S}_{11}'(s_1' + s_2') & \bar{S}_{11}'(r_1's_2' + r_2's_1') \\ \bar{S}_{22}' \dfrac{r_1's_2' + r_2's_1'}{[r_1'^2 + s_1'^2][r_2'^2 + s_2'^2]} & \bar{S}_{22}' \left(\dfrac{s_1'}{r_1'^2 + s_1'^2} + \dfrac{s_2'}{r_2'^2 + s_2'^2} \right) \end{bmatrix}^{(k)}, \tag{14}$$

so that (13a,b) may be recast as

$$b_i^{(k)'} = 2\sqrt{a^{(k)2} - x'^2}\, B_{ij}^{(k)'} \bar{\sigma}_{2j}'. \tag{15}$$

From eqn (14), it appears that $\mathbf{B}^{(k)'}$ is a *non-symmetric* matrix since the off-diagonal components $B_{12}^{(k)'}$ and $B_{21}^{(k)'}$ may not always be equal; see also eqns (14)–(15) in Sumarac and Krajcinovic (1989). This observation, however, is incorrect since it can be proved that $B_{12}^{(k)'} = B_{21}^{(k)'}$ is guaranteed for an open microcrack. To see this, we note that

$$r_1'^2 + s_1'^2 = (r_1' + is_1')(r_1' - is_1') = \lambda_1'\lambda_3' \tag{16a}$$

$$r_2'^2 + s_2'^2 = (r_2' + is_2')(r_2' - is_2') = \lambda_2'\lambda_4', \tag{16b}$$

where λ_3' and λ_4' are two complex roots of (12) conjugate to the roots λ_1' and λ_2', respectively. Since λ_1', λ_2', λ_3' and λ_4' are the roots of (12), they must satisfy

$$\lambda_1'\lambda_2'\lambda_3'\lambda_4' = \bar{S}_{22}'/\bar{S}_{11}'. \tag{17}$$

Therefore, we arrive at

$$(r_1'^2 + s_1'^2)(r_2'^2 + s_2'^2) = \bar{S}_{22}'/\bar{S}_{11}' \tag{18}$$

$$\bar{S}_{22}' \frac{r_1's_2' + r_2's_1'}{[r_1'^2 + s_1'^2][r_2'^2 + s_2'^2]} = \bar{S}_{11}'(r_1's_2' + r_2's_1'). \tag{19}$$

Hence, $B_{12}^{(k)'} = B_{21}^{(k)'}$ and $\mathbf{B}^{(k)'}$ is always *symmetric* for an open microcrack. For a *closed* microcrack under mode II *frictional* sliding, eqns (13a,b) and (14) must be appropriately modified; see Horii and Nemat-Nasser (1983, p. 162) for an approximate treatment. Essentially, one may set $B_{21}^{(k)'} = B_{22}^{(k)'} = b_2^{(k)'} = 0$, and replace $\bar{\sigma}_{22}'$ and $\bar{\sigma}_{21}'$ by $\bar{\sigma}_{22}' - \bar{\sigma}_{22}^c$ and $\bar{\sigma}_{21}' + \mu\,\mathrm{sgn}\,(\bar{\sigma}_{21}')\bar{\sigma}_{22}^c$, respectively. Here, μ is the coefficient of friction, and $\bar{\sigma}_{22}^c$ is the compressive normal stress transmitted across the closed crack [see eqn (28) in Horii and Nemat-Nasser (1983)]. Further, the matrix $\mathbf{B}^{(k)'}$ is *non-symmetric* as a direct consequence of frictional slip.

Using the fact that $n_1' = 0$ and eqns (7), (8) and (13a,b), we arrive at

$$S_{11}^{\mathrm{II}(k)'} = S_{12}^{\mathrm{II}(k)'} = S_{21}^{\mathrm{II}(k)'} = S_{13}^{\mathrm{II}(k)'} = S_{31}^{\mathrm{II}(k)'} = 0 \tag{20a}$$

$$S_{22}^{\mathrm{II}(k)'} = \frac{\pi a^{(k)2}}{A} \left(\frac{s_1'}{r_1'^2 + s_1'^2} + \frac{s_2'}{r_2'^2 + s_2'^2} \right) \bar{S}_{22}' = \frac{\pi a^{(k)2}}{A} B_{22}^{(k)'} \tag{20b}$$

$$S_{33}^{\mathrm{II}(k)'} = \frac{\pi a^{(k)2}}{A} (s_1' + s_2') \bar{S}_{11}' = \frac{\pi a^{(k)2}}{A} B_{11}^{(k)'} \tag{20c}$$

$$S_{23}^{\mathrm{II}(k)'} = \frac{\pi a^{(k)2}}{A} \frac{r_1's_2' + r_2's_1'}{[r_1'^2 + s_1'^2][r_2'^2 + s_2'^2]} \bar{S}_{22}' = \frac{\pi a^{(k)2}}{A} B_{21}^{(k)'} \tag{20d}$$

$$S_{32}^{\mathrm{II}(k)'} = \frac{\pi a^{(k)2}}{A} (r_1's_2' + r_2's_1') \bar{S}_{11}' = \frac{\pi a^{(k)2}}{A} B_{12}^{(k)'}. \tag{20e}$$

where $S_{ij}^{d(k)}$ denotes the kth microcrack-induced "additional inelastic compliance". From eqns (20d, e), it is realized that $S_{21}^{d(k)} = S_{12}^{d(k)}$ for an open microcrack. By contrast, $S_{22}^{d(k)} = S_{23}^{d(k)} = 0$ and $S_{23}^{d(k)} \neq S_{32}^{d(k)}$ for a closed sliding microcrack [see eqn (32) in Horii and Nemat-Nasser (1983)]. Thus, $\mathbf{S}^{d(k)}$ is *symmetric* and *non-symmetric*, respectively, for an *open* and a *closed* microcrack. In addition, the inelastic compliance $\mathbf{S}^{d}$ due to an ensemble of microcracks within a representative volume can be expressed as

$$S_{ij}^{d} = \sum_{k} g_{mi}^{(k)} g_{nj}^{(k)} S_{mn}^{d(k)} = \sum_{k} S_{ij}^{d(k)} = N\langle S_{ij}^{d(k)} \rangle \tag{21a}$$

in which N signifies the total number of active (open or sliding) microcracks per representative-volume surface, and $\langle \cdot \rangle$ represents the expected value. In the limit (a large number of microcracks per representative volume), the summation operator can be replaced by the integral operator over all active microcracks:

$$S_{ij}^{d} = N \int_{\Omega} S_{ij}^{d(k)} p(\theta, a)\, \mathrm{d}\Omega, \tag{21b}$$

where $p(\theta, a)$ is a joint probability density function of orientation and crack size, and Ω is the domain of all active microcracks. It is emphasized that $\mathbf{S}^{d}$ depends on the yet *unknown* elastic-damage secant compliance $\bar{\mathbf{S}}$. Consequently, the self-consistent method demands iterative schemes to solve strains and compliances. Since $\bar{\varepsilon} = \bar{\varepsilon}^{e} + \bar{\varepsilon}^{d}$, the elastic-damage secant compliance takes the form: $\bar{\mathbf{S}} = \mathbf{S}^{0} + \mathbf{S}^{d}(\bar{\mathbf{S}})$.

2.2.1. *Remark*. For mode II frictional sliding, secant compliance moduli are non-symmetric and hence eqns (11) (12) should not be used. Instead, according to (8) and (10), one should use the following equation to solve complex roots:

$$\bar{S}'_{11}\lambda'^{4} - (\bar{S}'_{13} + \bar{S}'_{31})\lambda'^{3} + (\bar{S}'_{12} + \bar{S}'_{21} + \bar{S}'_{33})\lambda'^{2} - (\bar{S}'_{23} + \bar{S}'_{32})\lambda' + \bar{S}'_{22} = 0. \tag{22}$$

That is, eqn (22) should be utilized in conjunction with eqns (20a–e) for open microcracks, and together with eqn (32) in Horii and Nemat-Nasser (1983) for closed microcracks, respectively. To carry out the self-consistent scheme, a general non-symmetric anisotropic matrix iteration algorithm is warranted. In addition, numerical integration scheme for (21b) is needed. These issues will be addressed in Section 4.

Moreover, the "thermodynamic force" conjugate to the "rate of change of the microcrack density" can be derived straightforwards. Let us define

$$S_{ij}^{*(k)} \equiv \frac{A}{\pi a^{(k)2}} S_{ij}^{d(k)} \quad \text{or} \quad S_{ij}^{d(k)} \equiv \frac{\pi a^{(k)2}}{A} S_{ij}^{*(k)} \tag{23}$$

where $i, j = 1, 2, 3$. In the spirit of thermodynamics, we may consider statistical area-average damage by treating $a^{(k)}$ and $\mathbf{n}^{(k)}$ as random variables (not necessarily perfectly random); see also Wu (1985). Therefore, the area-average values may be replaced by their appropriate *expected* values. Hence, we have

$$\langle \mathbf{S} \rangle = \mathbf{S}^{0} + \langle \mathbf{S}^{d} \rangle = \mathbf{S}^{0} + N\left\langle \frac{\pi a^{(k)2}}{A} \mathbf{S}^{*(k)} \right\rangle = \mathbf{S}^{0} + \langle \omega^{(k)} \mathbf{S}^{*(k)} \rangle, \tag{24}$$

in which $\omega^{(k)} \equiv N\pi a^{(k)2}/A$; i.e. the non-dimensional microcrack area-concentration parameter per unit surface (see Budiansky and O'Connell, 1976). The time derivative of (24) then yields (see also Wu, 1985)

$$\langle \dot{\mathbf{S}} \rangle = \langle \dot{\omega}^{(k)} \mathbf{S}^{*(k)} \rangle + \langle \omega^{(k)} \rangle \left\langle \frac{\partial \mathbf{S}^{*(k)}}{\partial \mathbf{S}} \right\rangle : \langle \dot{\mathbf{S}} \rangle. \tag{25}$$

Note that $\langle \dot{\omega}^{(k)} \rangle$ in general includes both effects of *initiation* of new microcracks ($\dot{N}$) and *growth* of existing microcracks ($\dot{a}$). From (25), we obtain

$$\langle \dot{\mathbf{S}} \rangle = \left[\mathbf{I} - \langle \omega^{(k)} \rangle \left\langle \frac{\partial \mathbf{S}^{*(k)}}{\partial \mathbf{S}} \right\rangle \right]^{-1} : \langle \dot{\omega}^{(k)} \rangle \langle \mathbf{S}^{*(k)} \rangle, \tag{26}$$

where $\mathbf{I}$ is the fourth-order identity tensor. Substitution of (26) into the damage dissipation inequality (4b) then leads to

$$\tfrac{1}{2} \bar{\boldsymbol{\sigma}} \left(\left[\mathbf{I} - \langle \omega^{(k)} \rangle \left\langle \frac{\partial \mathbf{S}^{*(k)}}{\partial \mathbf{S}} \right\rangle \right]^{-1} : \langle \dot{\omega}^{(k)} \rangle \langle \mathbf{S}^{*(k)} \rangle \right) : \bar{\boldsymbol{\sigma}} \geqslant 0, \tag{27}$$

where $\bar{\boldsymbol{\sigma}}$ is now a vector of three components $(\bar{\tau}_1, \bar{\tau}_2, \bar{\tau}_3)$ for a two-dimension case. From (27), it is observed that the "thermodynamic driving force" ξ conjugate to the rate of change of the microcrack area-concentration parameter $\langle \dot{\omega}^{(k)} \rangle$ is simply

$$\xi \equiv \tfrac{1}{2} \bar{\boldsymbol{\sigma}} : \left(\left[\mathbf{I} - \langle \omega^{(k)} \rangle \left\langle \frac{\partial \mathbf{S}^{*(k)}}{\partial \mathbf{S}} \right\rangle \right]^{-1} : \langle \mathbf{S}^{*(k)} \rangle \right) : \bar{\boldsymbol{\sigma}}. \tag{28}$$

The above result is at variance with that given in Wu (1985, eqn (38), i.e. $\xi \equiv \frac{1}{2} \bar{\boldsymbol{\sigma}} : \langle \mathbf{S}^{*(k)} \rangle : \bar{\boldsymbol{\sigma}}$). The latter work, although interesting and valuable, indeed misses some terms in (28) and hence results in some anomalies regarding thermodynamic "strain energy release rate density" ξ. For example, ξ given in Wu (1985) may *decrease* while $\bar{\boldsymbol{\varepsilon}}$ increases, thus predicting no further damage in the post-peak (softening) branch of the macroscopic stress–strain curve.

2.2.2. *Remark.* In the case of three-dimensional *isotropic* scalar damage, the damage tensor $\mathbf{D}$ reduces to a scalar variable d. By definition, the scalar damage variable d is the microcrack volume-concentration parameter $\langle \omega^{(k)} \rangle \equiv \langle N a^{(k)3} / V \rangle$. Therefore, we have (for three-dimensional elastic-damage):

$$\bar{\mathbf{S}} = \frac{1}{(1-d)} \mathbf{S}^0; \quad \mathbf{S}^d = \frac{d}{(1-d)} \mathbf{S}^0. \tag{29}$$

Analogous to (24), we can identify that

$$\langle \mathbf{S}^{*(k)} \rangle = \frac{1}{(1-d)} \mathbf{S}^0 = \langle \mathbf{S} \rangle. \tag{30}$$

Therefore, ξ defined in Wu (1985) renders

$$\xi = \tfrac{1}{2} \bar{\boldsymbol{\sigma}} : \langle \mathbf{S} \rangle : \bar{\boldsymbol{\sigma}} = \tfrac{1}{2} \bar{\boldsymbol{\sigma}} : \bar{\boldsymbol{\varepsilon}}, \tag{31}$$

while ξ given by (28) leads to

$$\xi = \tfrac{1}{2} \bar{\boldsymbol{\sigma}} : \frac{1}{(1-d)} \langle \mathbf{S} \rangle : \bar{\boldsymbol{\sigma}} = \tfrac{1}{2} \frac{\bar{\boldsymbol{\sigma}} : \bar{\boldsymbol{\varepsilon}}}{(1-d)}. \tag{32}$$

However, $\bar{\boldsymbol{\sigma}}/(1-d)$ is precisely the so-called "effective stress" $\tilde{\boldsymbol{\sigma}}$ (Kachanov, 1958). Denoting the undamaged virgin elastic stiffness by $\mathbf{C}^0$, we then arrive at

$$\xi = \tfrac{1}{2}\bar{\sigma} : \bar{\varepsilon} = \tfrac{1}{2}(\mathbf{C}^0 : \bar{\varepsilon}) : \bar{\varepsilon} \equiv \Psi^0(\bar{\varepsilon}) \tag{33}$$

where $\Psi^0(\bar{\varepsilon})$ is the undamaged strain energy density defined in Ju (1989).

3. MICROCRACK EVOLUTION EQUATIONS

It is likely that brittle materials (such as concrete, crystals, polycrystalline ceramics, etc.) have initial microcracks along some weak planes (e.g. the aggregate–cement interface in concrete) even before specimens are first loaded. Before the initial (existing) microcracks are arrested by some higher energy barriers (such as the cement paste in normal strength concrete), they propagate approximately along the same weak planes in a self-similar manner. The problem can be significantly simplified by assuming that activated initial microcracks grow to certain characteristic *final* lengths along weak planes (Zaitsev, 1983; Krajcinovic and Fanella, 1986). For example, initial microcracks on aggregate-cement interface planes of concrete may grow from $2a_0$ (initial crack length) to $2a_f$ (the aggregate facet size) in an unstable manner. Inevitably, there is randomness in initial and final microcrack lengths, orientations and center locations in brittle materials. As a consequence of the two-stage approximation of weak-plane microcrack lengths (either $2a_0$ or $2a_f$), the problem of keeping track of weak-plane microcrack growth in a representative volume reduces to a series of microcrack *stability* checks. Thus, classical fracture mechanics stability criteria can be used as tools to determine whether an initial microcrack will be *activated*. This procedure, nonetheless, *cannot* accommodate nucleation of new microcracks along different weak planes.

A microcrack kinetic algorithm based on fracture criteria (see, e.g. Krajcinovic and Fanella, 1987) is intrinsicly *stress-controlled*. This type of mechanism, however, can only depict the ascending portion of a macroscopic stress strain curve, not the descending ("softening") portion. Before a "point" on a stress–strain curve reaches the peak, a stress-controlled loading criterion is qualitatively equivalent to a strain-controlled one. In the "softening" branch, however, a stress-controlled loading criterion will not suffice since the stress level is *decreasing*. In fact, in the descending branch of a stress–strain curve, there must be significant number of microcrack *nucleations*, and hence the "cleavage 1" process assumption is no longer valid. These and related issues should be further investigated in the future.

Restricting our attention to the "cleavage 1" deformation processes in this work, we consider the following three types of damage modes under *biaxial* loadings: (1) mode I (open) microcrack growth only, (2) mode II (closed) microcrack growth only, and (3) mixed modes I and II (open/closed) microcrack growth. In particular, excellent mode I tensile damage kinetic equations were presented by Krajcinovic and Fanella (1986) and Sumarac and Krajcinovic (1987), whereas valuable mode II compressive damage kinetic equations were proposed by Fanella and Krajcinovic (1988). Their presentations were, nonetheless, restricted to *monotonically increasing* loading cases. Therefore, no unloading/reloading stress paths or microcrack opening/closing effects were permitted in their presentations. The restriction on status change from opening to closing (or vice versa) can be removed by checking the *sign* of individual local *normal* stress. The corresponding symmetric or non-symmetric damage-induced inelastic compliance components can be obtained from eqns (20a–e) for *open* microcracks, and from eqn (32) in Horii and Nemat-Nasser (1983) for *closed* microcracks. It is remarked that in general eqn (22) should be used to solve complex roots. On the other hand, the restriction on "monotonically increasing loads" can be removed by computing and checking whether there are *undergoing* microcrack growth (excluding those previously propagating and currently arrested microcracks). If there is no "angle fan" domain in which *additional* microcrack growth is now taking place, then the current incremental load step is in an *unloading* state. Therefore, "active microcrack growth" is the valid current loading condition, regardless of prior existence (or non-existence) of certain "angle fans" where microcracks previously experienced growth.

Accordingly, the additional inelastic compliance $\mathbf{S}^d$ takes the form:

$$\mathbf{S}^{d} = \mathbf{S}_{u}^{d} + \mathbf{S}_{i}^{d} + \mathbf{S}_{f}^{d} \tag{34}$$

where $\mathbf{S}_{u}^{d}$ denotes the compliance contribution from undergoing microcrack growth, $\mathbf{S}_{i}^{d}$ signifies the contribution from arrested microcracks having *initial* sizes $2a_{0}^{(k)}$, and $\mathbf{S}_{f}^{d}$ represents the contribution from arrested microcracks having *final* sizes $2a_{f}^{(k)}$ due to *previous* microcrack growth. In particular, if $\mathbf{S}_{u}^{d} = 0$, then the current load level is not high enough to cause further damage and therefore all existing microcracks are arrested. Finally, $\mathbf{S}^{d}$ is added to $\mathbf{S}^{0}$ to obtain the secant compliance $\bar{\mathbf{S}}$. In what follows, for computational simplicity, it is assumed that all initial and final microcracks are of uniform sizes $2a_{0}$ and $2a_{f}$, respectively. For non-uniform initial microcrack sizes, we refer to Krajcinovic and Fanella (1986). Microcrack kinking will be addressed in Section 3.3.

3.1.1. *Remark.* If all microcracks are open and arrested with non-uniform sizes, then overall loading and unloading responses are linear and reversible (but not perfectly elastic). By contrast, if some microcracks propagate, then the loading response is nonlinear. Moreover, in mode II or mixed mode I/II with friction, some microcracks may be open and some closed. Therefore, the resulting loading and unloading responses are *nonlinear* for either "process models" or "non-process models".

3.1.2. *Remark.* In the case of mixed mode I/II, the strain energy release rate G' for a microcrack along a weak plane should include both mode I contribution G'_{1} and mode II contribution G'_{2}. In terms of secant compliance, G' may be expressed as (Sih *et al.*, 1965; Rice, 1975; Sumarac and Krajcinovic, 1989):

$$G' = G'_{1} + G'_{2} = C_{ij}^{\prime(k)} K'_{i} K'_{j}; \quad i, j = 1, 2, \tag{35a}$$

$$[\mathbf{C}^{\prime(k)}] = \frac{1}{2}\begin{bmatrix} B'_{22} & B'_{21} \\ B'_{12} & B'_{11} \end{bmatrix}^{(k)}. \tag{35b}$$

Therefore, we have

$$G' = \tfrac{1}{2}[B_{22}^{\prime(k)} K_{\mathrm{I}}^{\prime 2} + (B_{21}^{\prime(k)} + B_{12}^{\prime(k)}) K'_{\mathrm{I}} K'_{\mathrm{II}} + B_{11}^{\prime(k)} K_{\mathrm{II}}^{\prime 2}]. \tag{35c}$$

It is noted that K'_{I} and K'_{II} represent the mode I and II stress intensity factors at a particular orientation, respectively. The expressions for $B_{ij}^{\prime(k)}$ are given in eqn (14) for an open microcrack, and in Horii and Nemat-Nasser (1983) for a closed microcrack. The computed G' value is then compared against a given mixed mode critical strain energy release rate G_{c} to determine whether a microcrack will propagate.

3.2. *Mode I microcrack growth*

Under uniaxial or biaxial tensile loads, microcracks primarily grow in "mode I" fashion. Let us define the (global, homogenized) axial tensile stress by $\bar{\tau}_{2} = q$ and the lateral tensile stress by $\bar{\tau}_{1} = q^{*}$, respectively. The normal stress $\bar{\tau}'_{2}$ on the face of a typical microcrack at angle θ then reads

$$\bar{\tau}'_{2} = q\cos^{2}\theta + q^{*}\sin^{2}\theta > 0. \tag{36}$$

According to eqn (35c), one should compute K'_{I}, K'_{II} and G' even in the case of uniaxial or biaxial tension. However, since "mode I" is the primary concern (Sumarac and Krajcinovic, 1987), it is computationally simpler to use the mode I fracture criterion. In addition, strictly speaking, the "stress intensity factor" used in the microcrack growth stability criterion should take into account direct microcrack interaction effects:

$$f = K_{\mathrm{I}}^{\prime\mathrm{eff}} - K_{\mathrm{IC}}^{0} = 0 \tag{37a}$$

where $K_{\mathrm{I}}^{\prime\mathrm{eff}}$ is the mode I *effective* stress intensity factor, and K_{IC}^{0} is the mode I critical stress

intensity factor for a weak plane. We refer to Horii and Nemat-Nasser (1985a) and Kachanov (1987) for the derivation of $K_{\mathrm{I}}^{\prime\mathrm{eff}}$ and $K_{\mathrm{II}}^{\prime\mathrm{eff}}$ for line microcracks under various geometric configurations. Alternatively, within the applicable range (moderate microcrack concentration) of the self-consistent method, one may employ the simple "single crack" stability criterion (Krajcinovic and Fanella, 1986):

$$f = K_{\mathrm{I}}^{\prime} - K_{\mathrm{IC}}^{\circ} = 0 \tag{37b}$$

where $K_{\mathrm{I}}^{\prime} = \tilde{\tau}_2^{\prime}\sqrt{\pi a_0}$ is the mode I stress intensity factor for a typical microcrack. Naturally, exact microcrack interaction effects on $K_{\mathrm{I}}^{\prime\mathrm{eff}}$ (or $K_{\mathrm{II}}^{\prime\mathrm{eff}}$) depend on exact microcrack geometries such as number of interacting cracks, relative center locations, relative spacing, relative orientations, inner-tip or outer-tip, etc. In practice, however, it is not feasible to keep track of microstructural configuration for each microcrack.

By using (37b), the mode I microcrack stability criterion can be recast as

$$f = \tilde{\tau}_2^{\prime}\sqrt{\pi a_0} - K_{\mathrm{IC}}^{\circ} = 0. \tag{38}$$

For computational simplicity, let us assume that the lateral tension q^* is constant and the axial tension q is bigger than q^*. The value of q does *not* have to be monotonically increasing as long as $q > q^*$; i.e. unloading paths are permitted. In particular, from eqns (36) and (38), we have

$$q = \frac{K_{\mathrm{IC}}^{\circ}}{\sqrt{\pi a_0}\cos^2\theta} - q^*\tan^2\theta. \tag{39a}$$

Clearly, the first cracks to become activated are those for which q is a minimum, and are oriented in the plane $\theta = 0$ given the assumption that $q^* < K_{\mathrm{IC}}^{\circ}\sqrt{\pi a_0}$. Therefore, the corresponding minimum value of q is

$$q(\theta = 0) \equiv q_0 = \frac{K_{\mathrm{IC}}^{\circ}}{\sqrt{\pi a_0}}. \tag{39b}$$

The microcrack growth kinetic sequence proceeds as follows. Note that $q^* < q_0$.

(a) As $q < q_0$, all microcracks are stable and of initial size. Since all microcracks are open, perfectly randomly oriented and of equal size, the overall response is isotropic. Though the response is linear and reversible under the present stress level, the material state is really *elastic-damage*. In fact, the current elastic-damage compliance $\tilde{\mathbf{S}}$ is bigger than the virgin undamaged elastic compliance $\mathbf{S}^{\circ}$.

(b) As $q = q_0 > q^*$, those microcracks in the plane $\theta = 0$ become unstable and increase their lengths from $2a_0$ to $2a_{\mathrm{f}}$. It is assumed that there exists a higher energy barrier in the matrix so that microcracks become arrested once they reach $2a_{\mathrm{f}}$.

(c) As $q \equiv q_1 > q_0$, microcracks in the angle domain $(-\theta_1, \theta_1)$ become activated and increase in size from $2a_0$ to $2a_{\mathrm{f}}$. The material behaves anisotropically and the elastic-damage compliance increases. θ_1 value depends on q_1, q_0 and q^*. Specifically, in view of eqns (38)-(39b), θ_1 can be obtained by solving

$$q_1\cos^2\theta_1 + q^*\sin^2\theta_1 = q_0. \tag{40}$$

Thus, we arrive at

$$\cos\theta_1 = \sqrt{(q_0 - q^*)/(q_1 - q^*)} \quad \text{or} \quad \pm\theta_1 = \cos^{-1}\left(\sqrt{(q_0 - q^*)/(q_1 - q^*)}\right). \tag{41}$$

The compliance contributions $\mathbf{S}_{\mathrm{u}}^{\mathrm{d}}$ and $\mathbf{S}_{\mathrm{t}}^{\mathrm{d}}$ in eqn (34) can be computed (integrated) through eqns (20a–e) and (21b):

$$\mathbf{S}_u^d = \frac{N}{\pi}\int_{-\theta_1}^{\theta_1} \mathbf{g}^{(k)T}\mathbf{S}^{d(k)'}(\theta, a_f)\mathbf{g}^{(k)}\,d\theta \tag{42}$$

$$\mathbf{S}_i^d = \frac{N}{\pi}\int_{\pm\theta_1}^{\pm\pi/2} \mathbf{g}^{(k)T}\mathbf{S}^{d(k)'}(\theta, a_0)\mathbf{g}^{(k)}\,d\theta \tag{43}$$

where $1/\pi$ is the assumed *uniform* probability density function of microcrack orientation. Certainly, other probability density functions may be used when appropriate. For notational compactness, the integration bounds $(-\pi/2, -\theta_1)$ and $(\theta_1, \pi/2)$ are written together in (43) and in what follows. Readers should interpret the notation $(\pm\theta_1, \pm\pi/2)$ as the sum of two integration domains: $(-\pi/2, -\theta_1)$ and $(\theta_1, \pi/2)$. Note that eqns (42) and (43) are somewhat at variance with eqn (39) in Sumarac and Krajcinovic (1987) and eqn (55) in Sumarac and Krajcinovic (1989).

(d) As $q_0 < q < q_1$, the *unloading* case is taking place. There is no further microcrack growth because the apparent "active angle fan" shrinks. Therefore, $\mathbf{S}_u^d = 0$. It is emphasized that the *actual* "angle fan" (featuring $2a_f$ size) does *not* reduce owing to the *irreversible* nature of damage. Therefore, the elastic-damage compliance remains its previous value.

(e) As $q > q_1$, more microcracks are activated. The "angle fan" domain $(-\theta, \theta)$ can be computed from (41), with q_1 replaced by q. However, only the microcracks within domains $(-\theta, -\theta_1)$ and (θ_1, θ) are actually experiencing *unstable* growth. Hence, the compliance contribution $\mathbf{S}_u^d$ should be obtained from (20a–e) and (21b) with $(-\theta, -\theta_1)$ and (θ_1, θ) as integration bounds:

$$\mathbf{S}_u^d = \frac{N}{\pi}\int_{\pm\theta_1}^{\pm\theta} \mathbf{g}^{(k)T}\mathbf{S}^{d(k)'}(\tilde{\theta}, a_f)\mathbf{g}^{(k)}\,d\tilde{\theta}. \tag{44}$$

In addition, $\mathbf{S}_i^d$ and $\mathbf{S}_f^d$ in (34) now take the form:

$$\mathbf{S}_i^d = \frac{N}{\pi}\int_{\pm\theta}^{\pm\pi/2} \mathbf{g}^{(k)T}\mathbf{S}^{d(k)'}(\tilde{\theta}, a_0)\mathbf{g}^{(k)}\,d\tilde{\theta} \tag{45}$$

$$\mathbf{S}_f^d = \frac{N}{\pi}\int_{-\theta_1}^{\theta_1} \mathbf{g}^{(k)T}\mathbf{S}^{d(k)'}(\tilde{\theta}, a_f)\mathbf{g}^{(k)}\,d\tilde{\theta}. \tag{46}$$

(f) At some higher stress level $q = q_c$, K_I at $\theta = 0$ reaches the critical stress intensity factor K_{IC}^c of the matrix energy barrier. Therefore, microcracks having size $2a_f$ will resume to propagate through the matrix, and eventually lead to final failure:

$$q_c = \frac{K_{IC}^c}{\sqrt{\pi a_f}}. \tag{47}$$

As was commented by Sumarac and Krajcinovic (1987), the above scheme implicitly assumes that ultimate failure prefers "runaway cracks" in comparison with "localization modes". Numerical simulations by using both the self-consistent method and the "Taylor's model" will be given in Section 4.2.

3.3. *Mode II microcrack growth*

Under uniaxial or biaxial *compressive* loads, microcracks are closed and primarily grow in "mode II" fashion. Fanella and Krajcinovic (1988) proposed excellent kinetic equations for flat penny-shaped interface microcracks in concrete under mode II growth by using the "Taylor's model"; i.e. microcrack interaction effects are completely ignored. Our procedure here basically follows their treatment. However, the self-consistent method is employed here and weak microcrack interaction is taken into account through the

damage-induced stiffness degradation and anisotropy. Mode II microcrack kinking into brittle matrix is considered in Section 3.4. Further, microcracks under consideration are line microcracks instead of penny-shaped microcracks. It is also noted that unloading reloading is permitted in our treatment.

In accordance with eqn (35c), the mixed mode fracture criterion should be used. Nonetheless, since there is no mode I action under uniaxial or biaxial compressive loads, it is equivalent to employ the mode II fracture criterion only. Consequently, K'_{II} (or K''^{eff}_{II}) will be compared against K^{o}_{IIC} for a microcrack to determine whether it will propagate or not. Further, due to frictional sliding of closed microcracks, eqn (22) should be utilized to solve complex roots of characteristic equations; see Remark 2.2.1.

Let us denote by q and q^* the axial and lateral compressive stresses, respectively. q^* is assumed to be constant and $q > q^*$. The normal stress σ_n and shear stress τ_n on the face of a typical microcrack at angle θ are (Fanella and Krajcinovic, 1988):

$$\sigma_n = \bar{\tau}'_2 = q\cos^2\theta + q^*\sin^2\theta > 0 \tag{48}$$

$$\tau_s = \bar{\tau}'_1 - \mu\bar{\tau}'_2 = F(\theta)\left[q - \left(1 + \frac{\mu}{F(\theta)}\right)q^*\right], \tag{49}$$

where compression is taken as positive and $F(\theta) \equiv \pm\sin\theta\cos\theta - \mu\cos^2\theta$. According to Coulomb's law of friction, microcrack surfaces will slide relative to each other when $\tau_s \geqslant 0$ is met. Therefore, (49) can be solved for the upper and lower bounds ($\pm\theta_{s2}$ and $\pm\theta_{s1}$) of microcrack *orientations* for given values of q and q^*:

$$\tan(\pm\theta_{s1,s2}) = \frac{1 \pm \sqrt{1 - 4C_1(C_1+\mu)}}{2C_1}, \quad q \geqslant [2\mu(\sqrt{\mu^2+1}+\mu)+1]q^*, \tag{50}$$

where $C_1 \equiv \mu q^*/(q - q^*)$. Only those microcracks within ($\pm\theta_{s1}$, $\pm\theta_{s2}$) will experience relative frictional slip on their faces. Note that if $q^* = 0$ (uniaxial compression) or if $q \to \infty$, then $F(\theta) = 0$ and $\theta_{s1} = \tan^{-1}\mu$, $\theta_{s2} = \pi/2$. That is, microcracks within the fan ($-\tan^{-1}\mu$, $\tan^{-1}\mu$) will never slide and therefore will not contribute to S^{sl}.

A microcrack with relative sliding faces will exhibit mode II microcrack growth once its crack tip stress intensity factor K'_{II} (or K''^{eff}_{II}) reaches the critical value K^{o}_{IIC} along a weak plane. Accordingly, the mode II stability criterion can be expressed as

$$\tau_s = \frac{K^{o}_{IIC}}{\sqrt{\pi a_0}}. \tag{51}$$

From (49) and (51), we can solve for the q value needed to activate unstable mode II microcrack growth from $2a_0$ to $2a_f$ at a specific orientation θ:

$$q = \frac{K^{o}_{IIC}}{\sqrt{\pi a_0}F(\theta)} + \left(1 + \frac{\mu}{F(\theta)}\right)q^*. \tag{52}$$

As in the previous section, an unstable microcrack propagation will be arrested by the matrix having a higher critical stress intensity factor K^{o}_{IIC}. Again, the first microcracks to increase in size are those for which q is a minimum. Thus, critical angles $\pm\theta_0$ for the first microcrack growth are (Fanella and Krajcinovic, 1988):

$$\pm\theta_0 = \pm\tan^{-1}(\mu + \sqrt{\mu^2+1}). \tag{53}$$

The corresponding threshold value of q_0 is

$$q_0 = \frac{K_{IIC}^0}{\sqrt{\pi a_0} F(\theta_0)} + \left(1 + \frac{\mu}{F(\theta_0)}\right) q^*. \tag{54}$$

Therefore, mode II microcrack kinetic sequence is as follows.

(a) As $q < q_0$, no microcracks will increase in size. Nevertheless, microcracks oriented within the "angle fans" ($\pm\theta_{s1}$, $\pm\theta_{s2}$) will *slide*.

(b) As $q = q_0$, those microcracks in the plane $\pm\theta_0$ become unstable and change their lengths from $2a_0$ to $2a_f$.

(c) As $q \equiv q_1 > q_0$, microcracks within the "angle fans" ($\pm\theta_{u1}$, $\pm\theta_{u2}$) become unstable and grow $2a_0$ to $2a_f$. The sliding "angle fans" ($\pm\theta_{s1}$, $\pm\theta_{s2}$) also increase. The values of ($\pm\theta_{u1}$, $\pm\theta_{u2}$) can be obtained from eqn (52):

$$\tan(\pm\theta_{u1,u2}) = \pm\left\{\frac{1 \pm \sqrt{1 - 4C_2(C_2+\mu)}}{2C_2}\right\}, \quad q \geqslant q_0 \tag{55}$$

where $C_2 \equiv \{[K_{IIC}^0/\sqrt{\pi a_0}] + \mu q^*\}/(q - q^*)$. Since all microcracks are *closed*, the "displacement transformation matrix" $\mathbf{B}^{(k)}$ in eqn (14) must be modified. Specifically, $B_{21}^{(k)}$ and $B_{22}^{(k)}$ are set to 0, while $B_{12}^{(k)}$ and $B_{11}^{(k)}$ are available from eqn (32) in Horii and Nemat-Nasser (1983) together with eqn (22) in Remark 2.2.1. The inelastic compliance $\mathbf{S}_t^d$ attributable to stable *sliding* microcracks having initial size $2a_0$ can be computed as follows:

$$\mathbf{S}_t^d = \frac{N}{\pi}\left[\int_{\pm\theta_{s1}}^{\pm\theta_{u1}} \mathbf{g}^{(k)T}\mathbf{S}^{d(k)'}(\theta, a_0)\mathbf{g}^{(k)}\,d\theta + \int_{\pm\theta_{u2}}^{\pm\theta_{s2}} \mathbf{g}^{(k)T}\mathbf{S}^{d(k)'}(\theta, a_0)\mathbf{g}^{(k)}\,d\theta\right]. \tag{56}$$

Further, $\mathbf{S}_u^d$ in (34) reads

$$\mathbf{S}_u^d = \frac{N}{\pi}\int_{\pm\theta_{u1}}^{\pm\theta_{u2}} \mathbf{g}^{(k)T}\mathbf{S}^{d(k)'}(\theta, a_f)\mathbf{g}^{(k)}\,d\theta. \tag{57}$$

(d) As $q_0 < q < q_1$, the *unloading* case occurs. Therefore, $\mathbf{S}_u^d = 0$ and

$$\mathbf{S}_t^d = \mathbf{S}_u^d|_{old} = \frac{N}{\pi}\int_{\pm\theta_{u1,old}}^{\pm\theta_{u2,old}} \mathbf{g}^{(k)T}\mathbf{S}^{d(k)'}(\theta, a_f)\mathbf{g}^{(k)}\,d\theta, \tag{58}$$

where ($\pm\theta_{u1,old}$, $\pm\theta_{u2,old}$) is the *previous* range of unstable microcrack growth (assuming sliding). The domain of sliding microcracks also reduces and the *new* values of $\pm\theta_{s1}$ and $\pm\theta_{s2}$ may be obtained from (50). Hence, it follows that

$$\mathbf{S}_t^d = \frac{N}{\pi}\left[\int_{\pm\theta_{s1,new}}^{\pm\theta_{u1,old}} \mathbf{g}^{(k)T}\mathbf{S}^{d(k)'}(\theta, a_0)\mathbf{g}^{(k)}\,d\theta + \int_{\pm\theta_{u2,old}}^{\pm\theta_{s2,new}} \mathbf{g}^{(k)T}\mathbf{S}^{d(k)'}(\theta, a_0)\mathbf{g}^{(k)}\,d\theta\right]. \tag{59}$$

It is noted that the value of $\mathbf{S}_t^d$ is smaller than its previous value given by (56) because the sliding domain shrinks. As a consequence, the unloading compliance is *smaller* than its previous value.

(e) As $q > q_1$, more microcracks are activated. Both new sliding and unstable angle domains, ($\pm\theta_{s1}$, $\pm\theta_{s2}$) and ($\pm\theta_{u1}$, $\pm\theta_{u2}$), increase. The corresponding $\mathbf{S}_t^d$ and $\mathbf{S}_u^d + \mathbf{S}_f^d$ can be computed by using (56) and (57), respectively.

3.4. *Mixed mode I–II microcrack growth*

Under combined tensile and compressive loads, some microcracks are closed while others are open. In addition, some open microcracks may become closed during loading/unloading processes. Open microcracks grow in mixed mode fashion whereas closed

microcracks grow in "mode II" manner. The mixed mode fracture criterion given in eqn (35c) is used to determine microcrack stability. To facilitate numerical analysis, however, it is further assumed that the cross term $(B_{21}^{(k)}+B_{12}^{(k)})K_{\mathrm{I}}'K_{\mathrm{II}}'$ in (35c) can be neglected. Accordingly, (35c) can be recast as (Kanninen and Popelar, 1985):

$$\left(\frac{K_{\mathrm{I}}'}{K_{\mathrm{IC}}}\right)^2+\left(\frac{K_{\mathrm{II}}'}{K_{\mathrm{IIC}}}\right)^2=1, \tag{60a}$$

where K_{IC} and K_{IIC} denote critical stress intensity factors of a representative volume. Nonetheless, since all initial microcracks are assumed to be along weak planes, it is more rational to write

$$\left(\frac{K_{\mathrm{I}}'}{K_{\mathrm{IC}}^{\mathrm{o}}}\right)^2+\left(\frac{K_{\mathrm{II}}'}{K_{\mathrm{IIC}}^{\mathrm{o}}}\right)^2=1, \tag{60b}$$

where $K_{\mathrm{IC}}^{\mathrm{o}}$ and $K_{\mathrm{IIC}}^{\mathrm{o}}$ are critical stress intensity factors of weak planes. Again, it is emphasized that eqn (22) should be employed to solve complex roots.

Let us consider a typical combined loading case in which the axial *compressive* stress is denoted by q and the lateral *tensile* stress is denoted by q^*. Moreover, q^* is assumed to be constant (relatively small) while q is varying from 0 to a certain value. Due to obvious symmetry of the problem, we will derive formulas only for θ within the $(0, \pi/2)$ domain. During actual numerical integration of compliance components, however, both positive and negative θ bounds should be included. The stresses $\sigma_n\,(=\bar{\tau}_2')$ and $\bar{\tau}_1'\,(=\bar{\sigma}_{12}')$ on the face of a typical microcrack at angle θ are

$$\sigma_n=\bar{\tau}_2'=-q\cos^2\theta+q^*\sin^2\theta \tag{61}$$

$$\bar{\tau}_3'=(-q-q^*)\sin\theta\cos\theta \tag{62}$$

where tension is taken as positive. The "angle boundary" separating the domains of *open* and *closed* microcracks can be found by setting $\sigma_n=0$. Hence, we obtain

$$\tan^2\theta_{\mathrm{b}}=\frac{q}{q^*};\quad \theta_{\mathrm{b}}=\tan^{-1}(\sqrt{q/q^*}). \tag{63}$$

The upper and lower bounds for open microcracks are $\pi/2$ and θ_{b}, respectively.

For *closed* microcracks ($\sigma_n<0$), the sliding shear stress reads

$$\tau_{\mathrm{s}}=\bar{\tau}_3'-\mu\bar{\tau}_2'=-F(\theta)\left[q+\left(1+\frac{\mu}{F(\theta)}\right)q^*\right], \tag{64}$$

where $F(\theta)\equiv\sin\theta\cos\theta-\mu\cos^2\theta$. The criterion for microcrack surface-sliding is

$$\tau_{\mathrm{s}}=-(q+q^*)\sin\theta\cos\theta+\mu(q\cos^2\theta-q^*\sin^2\theta)\leqslant 0. \tag{65}$$

The θ-bound can be obtained by setting $\tau_{\mathrm{s}}=0$:

$$\tan\theta_{\mathrm{s}}=\frac{-1\pm\sqrt{1+4H_1(\mu-H_1)}}{2H_1}, \tag{66a}$$

where $H_1\equiv\mu q^*/(q+q^*)$. Since we require that $\theta_{\mathrm{s}}>0$, there should exist only one θ_{s}:

$$\theta_s = \tan^{-1}\left(\frac{-1+\sqrt{1+4H_1(\mu-H_1)}}{2H_1}\right). \tag{66b}$$

This θ_s value is, in fact, the *lower* angle bounds for closed microcrack sliding. The *upper* bound is simply θ_b given in (63) since sliding shear stress τ_s is negative at the θ_b plane. Only those microcracks within $(\pm\theta_s, \pm\theta_b)$ will exhibit relative frictional slip on their faces. Again, it is noted that as $q^* = 0$ (uniaxial compression) or as $q \to \infty$, then $F(\theta) = 0$ and $\theta_s = \tan^{-1}\mu$, $\theta_b = \pi/2$. As q increases from 0, θ_s and θ_b also increase but never exceed $\tan^{-1}\mu$ and $\pi/2$, respectively.

For closed microcracks, the mixed mode fracture criterion (60b) reduces to the mode II fracture criterion. Therefore, as in the previous section, a sliding microcrack will experience mode II microcrack growth once its crack tip stress intensity factor K'_{II} reaches the critical value K^o_{IIC} along a weak plane. Accordingly, mode II stability criterion requires the following loading level q for a specified θ

$$q = \frac{K^o_{IIC}}{\sqrt{\pi a_0}F(\theta)} - \left(1+\frac{\mu}{F(\theta)}\right)q^*. \tag{67}$$

The first microcracks to propagate are those for which q is a minimum:

$$\theta_0^{II} = \tan^{-1}(\mu+\sqrt{\mu^2+1}), \tag{68}$$

where it has been assumed that $\mu q^* \neq K^o_{IIC}/\sqrt{\pi a_0}$. If $\theta_0^{II} > \theta_b$ (opening/closing boundary), then set $\theta_0^{II} = \theta_b$. The corresponding threshold value of q_0^{II} is

$$q_0^{II} = \frac{K^o_{IIC}}{\sqrt{\pi a_0}F(\theta_0^{II})} - \left(1+\frac{\mu}{F(\theta_0^{II})}\right)q^*. \tag{69}$$

The mode II angle bounds for unstable weak-plane microcrack growth, $(\theta_{u1}^{II}, \theta_{u2}^{II})$, can be obtained from eqn (67):

$$\tan\theta_{u1,u2}^{II} = \frac{1\pm\sqrt{1-4H_2(H_2+\mu)}}{2H_2}, \quad (q+q^*)^2 \geqslant 4\left[\frac{K^o_{IIC}}{\sqrt{\pi a_0}}-\mu q^*\right]\left[\frac{K^o_{IIC}}{\sqrt{\pi a_0}}+\mu q\right], \tag{70a}$$

where $H_2 \equiv \{[K^o_{IIC}/\sqrt{\pi a_0}]-\mu q^*\}/(q+q^*)$. If $\mu q^* < K^o_{IIC}/\sqrt{\pi a_0}$ (typically), then there are two roots θ_{u1}^{II} and θ_{u2}^{II}. On the other hand, if $\mu q^* > K^o_{IIC}/\sqrt{\pi a_0}$ (unlikely), then there is only one root θ_u^{II}:

$$\tan\theta_u^{II} = \frac{1-\sqrt{1-4H_2(H_2+\mu)}}{2H_2}. \tag{70b}$$

Note that θ_{u1}^{II} and θ_{u2}^{II} (or simply θ_u^{II}) should fall within the sliding range (θ_s, θ_b); see Fig. 2 for a schematic plot.

For *open* microcracks, a mixed mode fracture criterion such as (70b) may be used to check microcracks stability. For convenience, let us define $\alpha \equiv K^o_{IIC}/K^o_{IC}$. Hence, (60b) can be rephrased as:

$$\alpha^2(K'_I)^2+(K'_{II})^2 = K^{o2}_{IIC}. \tag{71}$$

Substitution of (61), (62) into (71) then renders the microcrack stability condition:

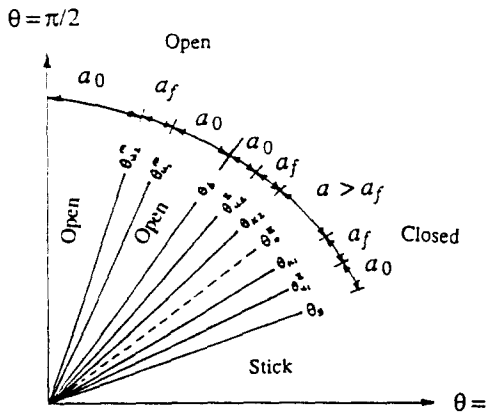

Fig. 2. An example of domains of mode II microcrack face sliding, unstable microcrack growth and mixed mode unstable microcrack growth. θ_b separates the open region from the closed region.

$$\alpha^2(-q\cos^2\theta+q^*\sin^2\theta)^2+(q+q^*)^2\sin^2\theta\cos^2\theta=\frac{K_{IIC}^{o2}}{\pi a_0}, \tag{72}$$

or, equivalently,

$$\left(\alpha^2q^{*2}-\frac{K_{IIC}^{o2}}{\pi a_0}\right)\tan^4\theta+\left(q^2+q^{*2}-6qq^*-2\frac{K_{IIC}^{o2}}{\pi a_0}\right)\tan^2\theta+\left(\alpha^2q^2-\frac{K_{IIC}^{o2}}{\pi a_0}\right)=0. \tag{73}$$

From (73), we can express q in terms of $\tan\theta$, q^*, α, and $K_{IIC}^{o2}/\pi a_0$ [analogous to (67)], and solve for threshold values θ_0^m and q_0^m corresponding to first microcracks to increase in size from $2a_0$ to $2a_f$ within $(\theta_b, \pi/2)$ domain.

In order to define the unstable "angle domain" for a given q value, we have to solve eqn (73). Obviously, (73) is amenable to exact solutions. Due to the constraint that $\theta > 0$, there are at most *two* real solutions to (73): θ_{u1}^m and θ_{u2}^m. We recall that the other two negative θ solutions will be accounted for during actual numerical integration of compliance components. These angle bounds should fall within the $(\theta_b, \pi/2)$ range. Otherwise, we should disregard θ_{u1}^m and/or θ_{u2}^m. In the event that both roots are feasible, then unstable open microcrack growth domain is defined by $(\theta_{u1}^m, \theta_{u2}^m)$ assuming that $q^* < K_{IC}^o/\sqrt{\pi a_0}$. If there is only *one* feasible root θ_u^m to (73), then the unstable growth domain is defined by (θ_b, θ_u^m) for open microcracks. See Fig. 2 for a schematic representation. Typically, $q_0^m < q_0^{II}$ and there is only one feasible root to (73).

Therefore, the mixed kinetic evolution for open and closed microcracks proceeds as follows.

(a) As $q < q_0^{II}$ and $q < q_0^m$, all microcracks are arrested. At the very beginning, $q = 0$ and $q^* > 0$, thus all microcracks are open. As q increases, some previously open microcracks become *closed*. Microcracks oriented within the "angle fans" $(\pm\theta_s, \pm\theta_b)$ will *slide* and therefore the overall response is nonlinear. Further, the "stick" domain increases as q increases.

(b) As $q = q_0^{II}$ or $q = q_0^m$, those microcracks in the plane $\pm\theta_0^{II}$ (closed) or $\pm\theta_0^m$ (open) become unstable and change their lengths from $2a_0$ to $2a_f$. Note that the mode II and mixed mode microcracks growth generally do not initiate at the same time.

(c) As $q \equiv q_1 > q_0^{II}$ or $q \equiv q_1 > q_0^m$, microcracks within the "angle fans" $(\pm\theta_{u1}^{II}, \pm\theta_{u2}^{II})$ or $(\pm\theta_{u1}^m, \pm\theta_{u2}^m)$ become activated. The sliding "angle fans" $(\pm\theta_s, \pm\theta_b)$ also increase. We refer to (66b), (70a, b) and (73) for these load-dependent angle values. For open microcracks, the "displacement transformation matrix" $\mathbf{B}^{(k)}$ is given in eqn (14). For closed microcracks, $\mathbf{B}^{(k)}$ is given in Horii and Nemat-Nasser (1983). It is important to recall that the resulting $\mathbf{S}^d$ and $\bar{\mathbf{S}}$ are non-symmetric in nature. The inelastic compliance $\mathbf{S}_i^{dII}$ attributable to stable mode II *sliding* microcracks having initial size $2a_0$ can be computed by

$$\mathbf{S}_i^{dII} = \frac{N}{\pi}\left[\int_{\pm\theta_s}^{\pm\theta_{u1}^{II}} \mathbf{g}^{(k)T}\mathbf{S}^{d(k)'}(\theta, a_0)\mathbf{g}^{(k)}\,d\theta + \int_{\pm\theta_{u2}^{II}}^{\pm\theta_b} \mathbf{g}^{(k)T}\mathbf{S}^{d(k)'}(\theta, a_0)\mathbf{g}^{(k)}\,d\theta\right] \tag{74}$$

while $\mathbf{S}_u^{dII}$ due to unstable closed microcracks can be obtained by

$$\mathbf{S}_u^{dII} = \frac{N}{\pi}\int_{\pm\theta_{u1}^{II}}^{\pm\theta_{u2}^{II}} \mathbf{g}^{(k)T}\mathbf{S}^{d(k)'}(\theta, a_f)\mathbf{g}^{(k)}\,d\theta. \tag{75}$$

In addition, $\mathbf{S}_i^{dm}$ attributable to stable mixed mode open microcracks having initial size $2a_0$ takes the form

$$\mathbf{S}_i^{dm} = \frac{N}{\pi}\left[\int_{\pm\theta_b}^{\pm\theta_{u1}^{m}} \mathbf{g}^{(k)T}\mathbf{S}^{d(k)'}(\theta, a_0)\mathbf{g}^{(k)}\,d\theta + \int_{\pm\theta_{u2}^{m}}^{\pm\pi/2} \mathbf{g}^{(k)T}\mathbf{S}^{d(k)'}(\theta, a_0)\mathbf{g}^{(k)}\,d\theta\right], \tag{76}$$

while $\mathbf{S}_u^{dm}$ attributable to unstable open microcracks can be obtained by

$$\mathbf{S}_u^{dm} = \frac{N}{\pi}\int_{\pm\theta_{u1}^{m}}^{\pm\theta_{u2}^{m}} \mathbf{g}^{(k)T}\mathbf{S}^{d(k)'}(\theta, a_f)\mathbf{g}^{(k)}\,d\theta. \tag{77}$$

If there is only one feasible root to (73), the integration limits in (76) and (77) should be replaced by $(\pm\theta_u^m, \pm\pi/2)$ and $(\pm\theta_b, \pm\theta_u^m)$, respectively.

(d) As $q_0 < q < q_1$, the *unloading* case occurs and $\mathbf{S}_u^{dII} = \mathbf{S}_u^{dm} = 0$. Further, for sliding closed microcracks, we have

$$\mathbf{S}_f^{dII} = \mathbf{S}_u^{dII}|_{old} = \frac{N}{\pi}\int_{\pm\theta_{u1,old}^{II}}^{\pm\theta_{u2,old}^{II}} \mathbf{g}^{(k)T}\mathbf{S}^{d(k)'}(\theta, a_f)\mathbf{g}^{(k)}\,d\theta \tag{78}$$

where $(\pm\theta_{u1,old}^{II}, \pm\theta_{u2,old}^{II})$ are the *old* ranges of mode II unstable microcrack growth at the *previous* load step. Note that if $\theta_{u2,old}^{II} > \theta_{b,new}$, then $\theta_{u2,old}^{II}$ in (78) should be replaced by $\theta_{b,new}$ since some microcracks now become open and the corresponding compliance contribution should belong to open (mixed mode) region. The domain of sliding closed microcracks also reduces and the *new* values of $\pm\theta_s$ may be obtained from (66b). Hence, it follows that

$$\mathbf{S}_i^{dII} = \frac{N}{\pi}\left[\int_{\pm\theta_{s,new}}^{\pm\theta_{u1,old}^{II}} \mathbf{g}^{(k)T}\mathbf{S}^{d(k)'}(\theta, a_0)\mathbf{g}^{(k)}\,d\theta + \int_{\pm\theta_{u2,old}^{II}}^{\pm\theta_{b,new}} \mathbf{g}^{(k)T}\mathbf{S}^{d(k)'}(\theta, a_0)\mathbf{g}^{(k)}\,d\theta\right]. \tag{79}$$

For open microcracks, we have

$$\mathbf{S}_f^{dm} = \mathbf{S}_u^{dm}|_{old} = \frac{N}{\pi}\int_{\pm\theta_{u1,old}^{m}}^{\pm\theta_{u2,old}^{m}} \mathbf{g}^{(k)T}\mathbf{S}^{d(k)'}(\theta, a_f)\mathbf{g}^{(k)}\,d\theta, \tag{80}$$

where $(\pm\theta_{u1,old}^{m}, \pm\theta_{u2,old}^{II})$ is the *old* range of mixed mode unstable microcrack growth at the *previous* load step. We have assumed that $\theta_{u2,old}^{II} < \theta_{b,new}$. The domain of open microcracks increases and therefore $\mathbf{S}_i^{dm}$ should be updated:

$$\mathbf{S}_i^{dm} = \frac{N}{\pi}\left[\int_{\pm\theta_{b,new}}^{\pm\theta_{u1,old}^{m}} \mathbf{g}^{(k)T}\mathbf{S}^{d(k)'}(\theta, a_0)\mathbf{g}^{(k)}\,d\theta + \int_{\pm\theta_{u2,old}^{m}}^{\pm\pi/2} \mathbf{g}^{(k)T}\mathbf{S}^{d(k)'}(\theta, a_0)\mathbf{g}^{(k)}\,d\theta\right] \tag{81}$$

(e) As $q > q_1$, more microcracks are activated. The mode II sliding and unstable angle domains, $(\pm\theta_s, \pm\theta_b)$ and $(\pm\theta_{u1}^{II}, \pm\theta_{u2}^{II})$, increase. Similarly, the mixed mode unstable angle domain, $(\pm\theta_{u1}^{m}, \pm\theta_{u2}^{m})$ or $(\pm\theta_b, \pm\theta_u^m)$ increases. The corresponding $\mathbf{S}_i^{dII}$, $[\mathbf{S}_u^{dII} + \mathbf{S}_f^{dII}]$, $\mathbf{S}_i^{dm}$ and $[\mathbf{S}_u^{dm} + \mathbf{S}_f^{dm}]$ values can be computed by using (74)–(77), respectively.

3.4.1. *Remark.* Mode II weak-plane (interface) microcracks having the size $2a_f$ are arrested by higher energy barrier of matrix material. However, if axial compressive stress is increased to a certain level, these microcracks may kink into brittle matrix in a stable fashion and eventually align with the axial compressive load direction; see, e.g. Nemat-Nasser and Horii (1982) and Horii and Nemat-Nasser (1985b, 1986). The kinking threshold stress q_{kink} can be obtained from [see, e.g. Zaitsev (1982, 1983)]:

$$q_{kink} = \frac{\sqrt{3}K_{IC}^c}{2\sqrt{\pi a_f}F(\theta_0^{II})} - \left(1 + \frac{\mu}{F(\theta_0^{II})}\right)q^*. \tag{82}$$

The angle bounds for initiation of stable kinked microcracks, $(\theta_{k1}, \theta_{k2})$, can be expressed analogous to (70a):

$$\tan\theta_{k1,k2} = \frac{1 \pm \sqrt{1-4H_3(H_3+\mu)}}{2H_3}, \quad (q+q^*)^2 \geqslant 4\left[\frac{\sqrt{3}K_{IC}^c}{2\sqrt{\pi a_f}} - \mu q^*\right]\left[\frac{\sqrt{3}K_{IC}^c}{2\sqrt{\pi a_f}} + \mu q\right] \tag{83}$$

where $H_3 \equiv \{[\sqrt{3}K_{IC}^c/2\sqrt{\pi a_f}] - \mu q^*\}/(q+q^*)$. For $\mu q^* < \sqrt{3}K_{IC}^c/2\sqrt{\pi a_f}$, there are two real roots. Note that θ_{k1} and θ_{k2} should fall within $(\theta_{u1}^{II}, \theta_{u2}^{II})$; see Fig. 2.

Assuming *stable* microcrack kinking, the "kink length" l can be related to the sliding shear stress τ_s; see, e.g. Zaitsev (1983), Horii and Nemat-Nasser (1986) and Fanella and Krajcinovic (1988). For cementitious composites below the brittle-ductile transition point, a simple formula may be used (Zaitsev, 1983):

$$l = \frac{4a_f^2\tau_s^2\cos^2\theta}{\pi K_{IC}^{c2}} \tag{84}$$

where τ_s is available from eqn (64). Finally, the additional compliance contribution $\mathbf{S}_{kink}^d$ due to kinked microcracks can be computed by

$$\mathbf{S}_{kink}^d = \frac{N}{\pi}\int_{\pm\theta_{k1}}^{\pm\theta_{k2}} \mathbf{g}^{(k)T}\mathbf{S}^{d(k)'}(\theta, l)\mathbf{g}^{(k)}\,d\theta. \tag{85}$$

4. COMPUTATIONAL ALGORITHMS AND NUMERICAL SIMULATIONS

In this section, computational algorithms are given for the proposed self-consistent damage models. In addition, three detailed numerical simulations are presented. These include a uniaxial tension test, a uniaxial compression test, and a tension/compression test of brittle materials. Due to a lack of *plane strain* experimental data at this stage, however, an actual experimental validation is not presented. Extensive experimental verification of the proposed models should be performed in the future. Nevertheless, the presented numerical simulations demonstrate the potential capability of the proposed micromechanical damage models to qualitatively explain and model physical behavior of brittle materials, without resorting to any fitted "material parameter" commonly utilized in phenomenological continuum damage models.

4.1. *Computational algorithms*

A self-consistent kinetic damage model naturally requires iterative schemes to obtain the yet *unknown* elastic-damage compliance $\bar{\mathbf{S}}$ corresponding to specified area-average stresses $\bar{\boldsymbol{\sigma}}$ or remote stresses $\boldsymbol{\sigma}^\infty$. As mentioned in Section 2.1, it is assumed that $\bar{\boldsymbol{\sigma}} \approx \boldsymbol{\sigma}^\infty$ in our problems. For mode I, mode II and mixed mode damage models discussed in Section 3, fortunately, the "sliding angles" $\pm\theta_s$, "unstable angles" $\pm\theta_u$ and "kink angles" $\pm\theta_k$ are *independent* of the iterative processes in finding compliances $\bar{\mathbf{S}}$ for sequentially applied loads

q. Therefore, the computational schemes involved in solving the proposed stress-controlled micromechanical damage models proceed as follows.

(1) For a given load q, compute "unstable angles" $\pm\theta_u$ according to (41) for mode I, (55) for mode II, as well as (70a, b) and (73) for mixed mode. "Sliding angles" $\pm\theta_s$ are computed according to (50) for mode II and (66b) for mixed mode. In addition, "kink angles" $\pm\theta_k$ are calculated according to (83). The "unstable" and "kink" angle domains should be stored as *history variables*. They depend on q only, independent of iterative steps in the following.

(2) Solve $\bar{\mathbf{S}}$ iteratively for a specified load q. The natural initial guess for the current $\bar{\mathbf{S}}$ is the *previous* secant compliance $\bar{\mathbf{S}}_{\text{old}}$. At the first loading step, we use the virgin elastic compliance $\mathbf{S}^0$ as an initial guess; see also Horii and Nemat-Nasser (1983, p. 168). For each trial compliance $\bar{\mathbf{S}}^{(n)}$, we have to solve eqn (22) so that displacement transformation matrix $\mathbf{B}^{(k)}$, crack opening displacements and inelastic compliance $\mathbf{S}^{d(k)}$ can be evaluated. As noted before, the secant compliance $\bar{\mathbf{S}}$ is in general a *non-symmetric* matrix when frictional sliding of microcrack faces is present. Equation (22) is simply a fourth order algebraic equation and is amenable to a closed-form exact solution. Further, we only need to solve (22) *once* (for each trial compliance $\bar{\mathbf{S}}^{(n)}$) at the orientation plane $\theta = 0$. For other orientations, the local roots λ_l' can be expressed by the roots λ_l at $\theta = 0$ (Lekhnitskii, 1950, p. 51):

$$\lambda_l' = \frac{\lambda_l \cos\theta - \sin\theta}{\cos\theta + \lambda_l \sin\theta}; \quad \bar{\lambda}_l' = \frac{\bar{\lambda}_l \cos\theta - \sin\theta}{\cos\theta + \bar{\lambda}_l \sin\theta} \tag{86}$$

where $\bar{\lambda}_l$ are the complex conjugate roots to λ_l. Once the roots of (22) in every desired orientation are obtained from closed-form solutions, $\mathbf{B}^{(k)}$, $\mathbf{S}^{d(k)}$ and $\mathbf{S}^{d(k)}$ for each microcrack contribution can be obtained from (9a), (14) and (20a–e) in Section 2.2, and from eqn (32) in Horii and Nemat-Nasser (1983).

(3) Obtain the damage-induced compliance $\mathbf{S}^d$ in (21b) by numerical integration. Here, we use Simpson's rule with 201 integration points at various orientations between $(-\pi/2, \pi/2)$. The compliance contributions $\mathbf{S}_u^d$, $\mathbf{S}_s^d$, $\mathbf{S}_f^d$ and $\mathbf{S}_{\text{kink}}^d$ can be computed by using (42)–(46) for mode I, (56)–(59) for mode II, (74)–(81) for mixed mode, and (82)–(85) for kinked microcracks.

(4) Obtain new trial compliance $\bar{\mathbf{S}}^{(n+1)}$ by adding $\mathbf{S}^d$ to $\mathbf{S}^0$. Compare this new trial compliance $\bar{\mathbf{S}}^{(n+1)}$ with the previous trial $\bar{\mathbf{S}}^{(n)}$. If the relative error is smaller than a preset tolerance, then the iterative process is said to be converged. On the other hand, if the relative error is unacceptable, then use $\bar{\mathbf{S}}^{(n+1)}$ as a new estimate, and go back to Step (2) to re-iterate until convergence is reached. This iterative procedure leads to superlinear rate of convergence, and typically requires only 5 to 7 iterations. The convergence criteria we employ here are based on L_2 and L_∞ norms. In particular, we check the following (TOL = 10^{-6}):

$$\frac{|\bar{\mathbf{S}}^{(n)} - \bar{\mathbf{S}}^{(n+1)}|_2}{|\bar{\mathbf{S}}^{(n+1)}|_\infty} \leqslant \text{TOL} \quad \text{or} \quad \frac{|\bar{\mathbf{S}}^{(n)} - \bar{\mathbf{S}}^{(n+1)}|_\infty}{|\bar{\mathbf{S}}^{(n+1)}|_\infty} \leqslant \text{TOL}. \tag{87}$$

If (87) is satisfied, then convergence is reached. Set $\bar{\mathbf{S}} \equiv \bar{\mathbf{S}}^{(n+1)}$ and go to Step (5).

(5) Apply the next load q_{new}. Set converged elastic-damage compliance $\bar{\mathbf{S}}$ in Step (4) to $\bar{\mathbf{S}}_{\text{old}}$ and go to Step (1).

4.2. *A uniaxial tension test*

A uniaxial tension test is considered in this section (see also Sumarac and Krajcinovic, 1987). For comparison purpose, the results of the self-consistent method are compared with those of Taylor's model. The virgin material is assumed to be isotropic linear elastic with Young's modulus $E^0 = 4000$ ksi (27 600 MPa) and $\nu^0 = 0.2$. Moreover, K_{IC}^0 is taken as 5 ksi-in.$^{1/2}$ (5.5 MN m$^{-3/2}$) and $a_0 = 0.6a_f$.

Two different initial microcrack area-concentration parameters are considered: $\omega_0 = 0.1131$ and 0.2262. Recall that by definition $\langle\omega\rangle = N\pi\langle a^2\rangle / A$. Although the maximum allowable value of ω is 1 for the self-consistent model, actual brittle materials fail at ω less than 1. At the beginning ($q \leqslant q_0$) and the asymptotic end ($q = \infty$) of the loading sequence, damaged materials are *isotropic* because microcrack orientations are perfectly random and microcrack sizes are uniform. Thus, both the self-consistent model and Taylor's model can be computed analytically for $q \leqslant q_0$ and $q = \infty$; see Horii and Nemat-Nasser (1983), and Sumarac and Krajcinovic (1987). The integration formulas for Taylor's model are analogous to the self-consistent model (42)–(46) with $\mathbf{S}^{d(k)}$ replaced by (plane strain condition):

$$S_{ij}^{d(k)} = \frac{2\pi a^2(1-\nu^{o2})}{AE^o}(\delta_{2i}\delta_{2j}+\delta_{3i}\delta_{3j}); \quad i,j = 1,2,3. \tag{88}$$

The relative difference in lateral compliances (dotted lines) and axial compliances (solid lines) between the self-consistent model and Taylor's model for two values of initial damage ω_0 are shown in Fig. 3a,b. Notice that the responses of two models are not equivalent even at $q/q_0 \leqslant 1$ due to initial (pre-existing) damage. It is also noted that as q approaches ∞ (not feasible), the final microcrack area-concentration parameters ω_f become 0.3142 and 0.6283, respectively. Further, the relative difference between the self-consistent model and Taylor's model depends on the degree of mean microcrack area-concentration $\langle\omega\rangle$. See Fig. 4a,b where the relative difference in compliances between the two models is plotted vs $\langle\omega\rangle$. For low damage concentration ($\langle\omega\rangle$ smaller than 27%), the relative difference in compliances is less than 10%; see Fig. 4a. For moderate damage ($\langle\omega\rangle$ between 27% to 45%), the relative difference ranges from 10% (at $q/q_0 \approx 1.04$) to approximately 30% (at $q/q_0 \approx 2.5$); see Fig. 4b. Thus, it appears that use of Taylor's model is acceptable for low damage concentration, in agreement with the finding reported in Sumarac and Krajcinovic (1987).

Figure 5a,b display normalized stresses versus normalized strains computed by the two models for the same two values of ω_0. Again, the relative difference is smaller than 10% for $\langle\omega\rangle$ less than 27%. In addition, the averaged stress–strain behavior is qualitatively reasonable for the self-consistent damage model. The ratios of $\bar{S}_{22}/\bar{S}_{11}$ versus the normalized axial stresses q/q_0 are exhibited in Fig. 6a,b. In Fig. 7a,b, the ratios $\bar{S}_{22}/\bar{S}_{11}$ are plotted against the microcrack area-concentration parameter $\langle\omega\rangle$.

4.3. *Uniaxial compression and biaxial tension/compression tests*

A uniaxial compression test and a biaxial tension/compression test are considered in this section. The virgin brittle composite material is assumed to be isotropic linear elastic with Young's modulus $E^o = 6000$ ksi (41 400 MPa) and $\nu^o = 0.2$. Fracture toughness properties of weak plane (interface) and matrix are taken to be $K_{IC}^o = 0.15$ ksi-in.$^{1/2}$ (0.165 MN m$^{-3/2}$), $K_{IIC}^o = 0.3$ ksi-in.$^{1/2}$ (0.33 MN m$^{-3/2}$), and $K_{IC}^o = 0.525$ ksi-in.$^{1/2}$ (0.578 MN m$^{-3/2}$). The initial and final microcrack lengths on weak planes are taken as $a_f = 0.375$ in. (0.953 cm) and $a_0 = 0.225$ in. (0.572 cm). The coefficient of friction on microcrack faces is 0.6. In addition, $q^* = 0$ for the uniaxial compression test, $q^* = 0.1$ ksi (0.69 MPa, tensile) for the biaxial test, and $\omega_0 = 0.2262$.

The axial load q is gradually increased from 0 to a certain peak value. For the uniaxial compression test, all microcracks are *closed* throughout the loading sequence. By contrast, for the tension/compression test, a small lateral tension is applied at the very beginning and all microcracks are initially *open*. As q increases, more and more microcracks change states from open to *closed*. Therefore, for the biaxial tension/compression test, some microcracks are open and grow in mixed mode, while others are closed and grow in mode II fashion during the loading sequence. After mode II microcracks kink into matrix material, however, kinked microcracks are considered as "tension cracks" and aligned with the axial loading direction. In both tests, kinked microcracks are assumed to grow in a *stable* fashion.

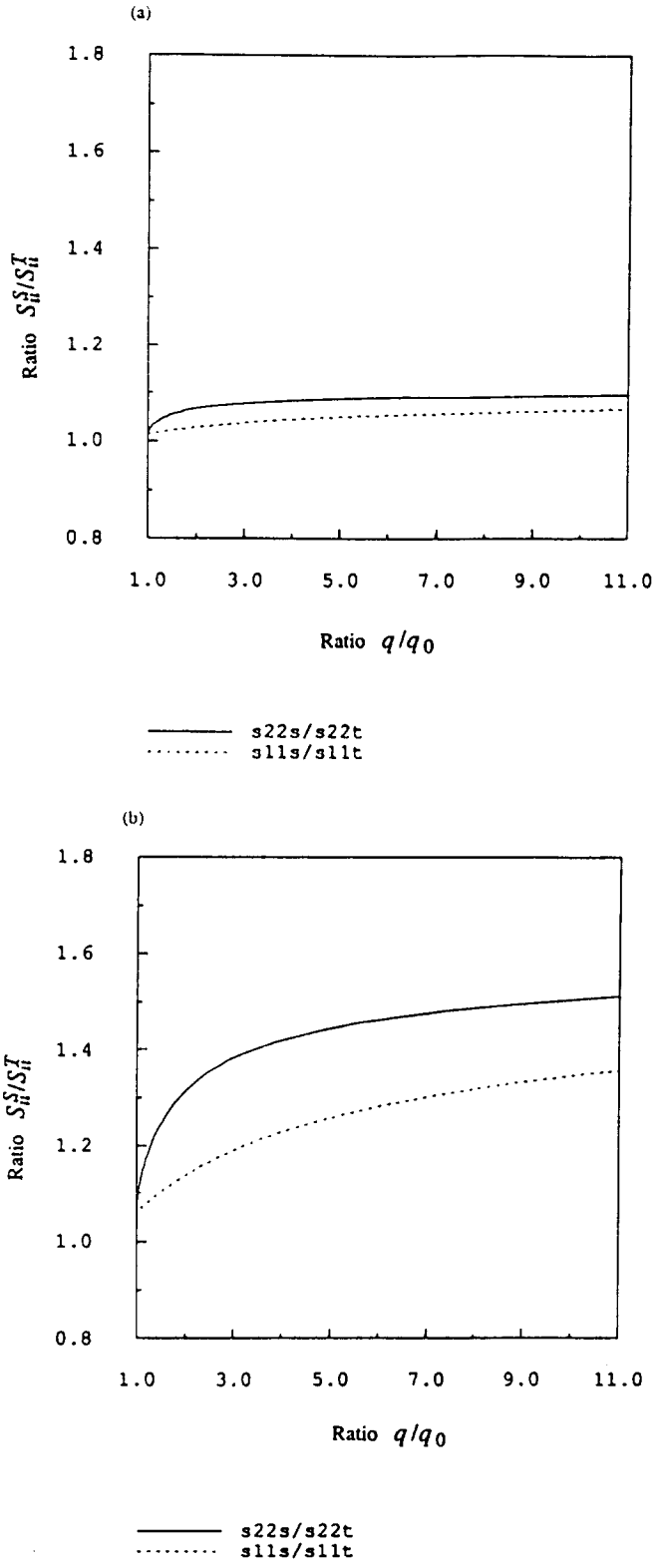

Fig. 3. The ratios of compliances computed by using the self-consistent and Taylor's models in axial (solid line) and lateral (dashed) directions vs the normalized stress q/q_0. Part (a) is for $\omega_0 = 0.1131$ and (b) for $\omega_0 = 0.2262$.

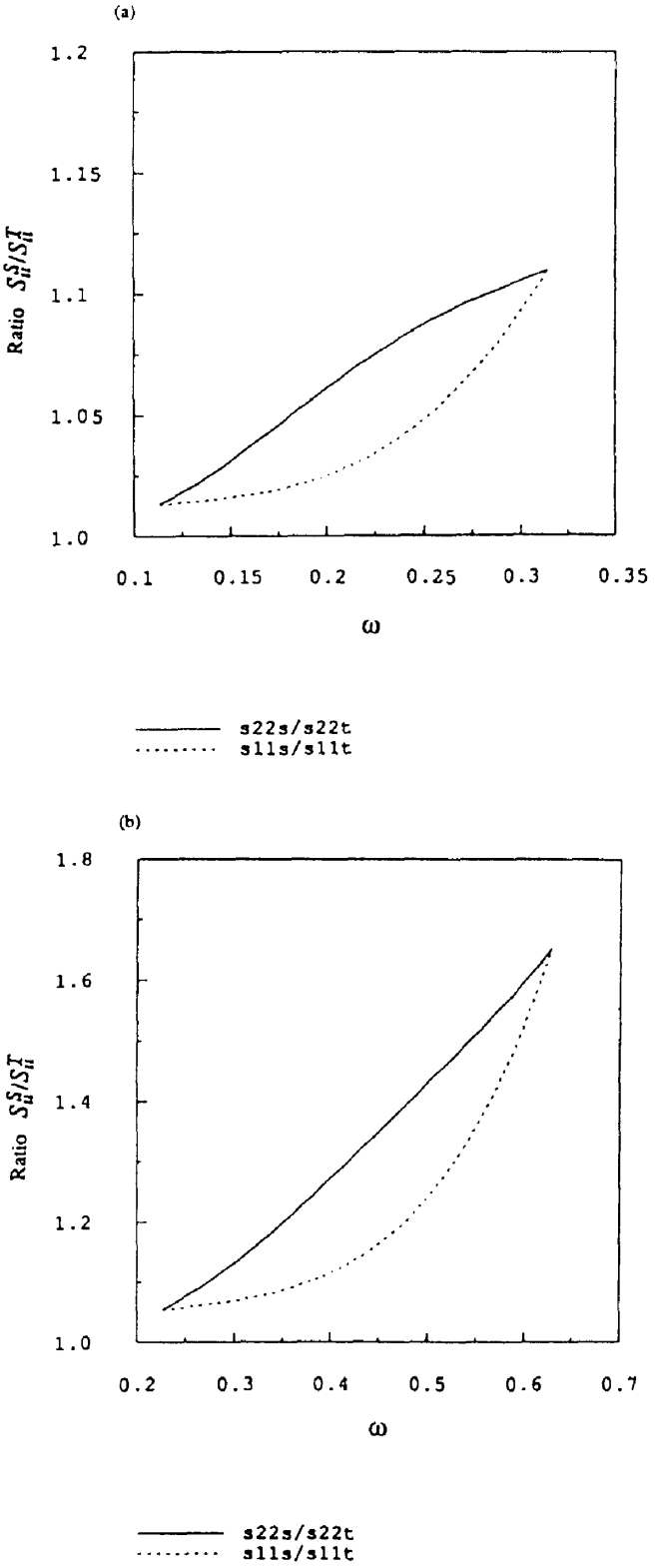

Fig. 4. The ratios of compliances computed by using the self-consistent and Taylor's models in axial and lateral directions vs the evolving microcrack concentration parameter ω for $\omega_0 = 0.1131$ (a) and 0.2262 (b), respectively.

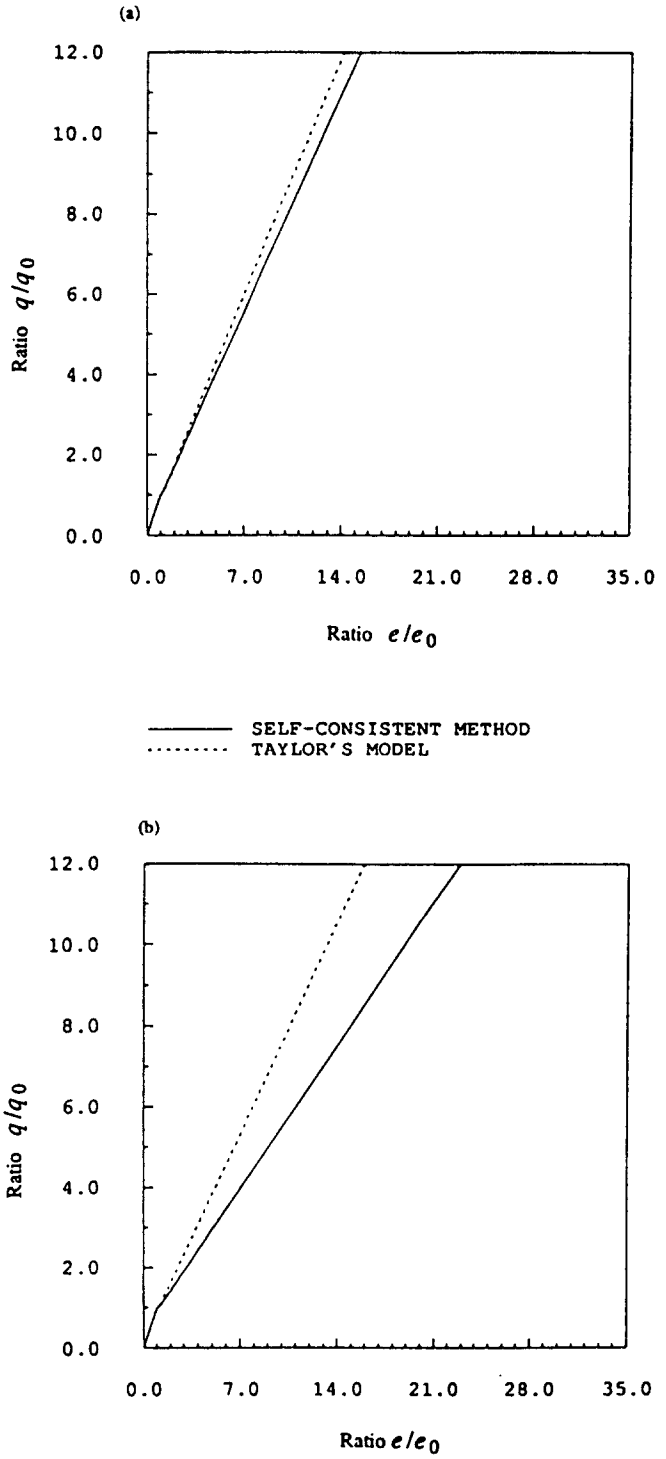

Fig. 5. The normalized stress vs the normalized strain computed by using the self-consistent and Taylor's models for $\omega_0 = 0.1131$ (a) and 0.2262 (b), respectively.

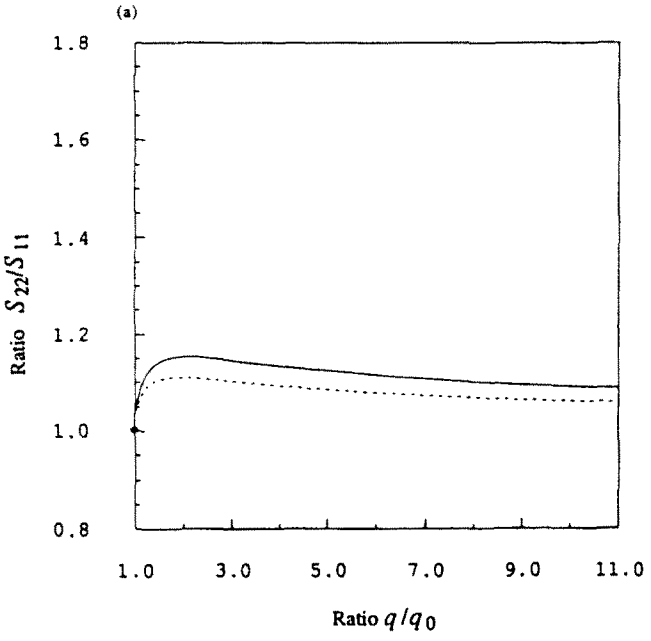

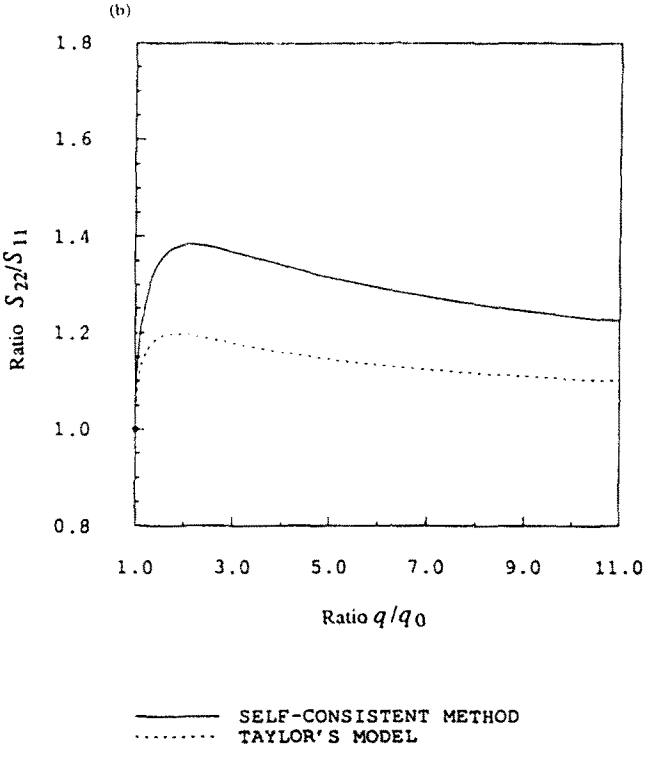

Fig. 6. S_{22}/S_{11} ratio vs the normalized stress computed by using the self-consistent and Taylor's models for $\omega_0 = 0.1131$ (a) and 0.2262 (b), respectively.

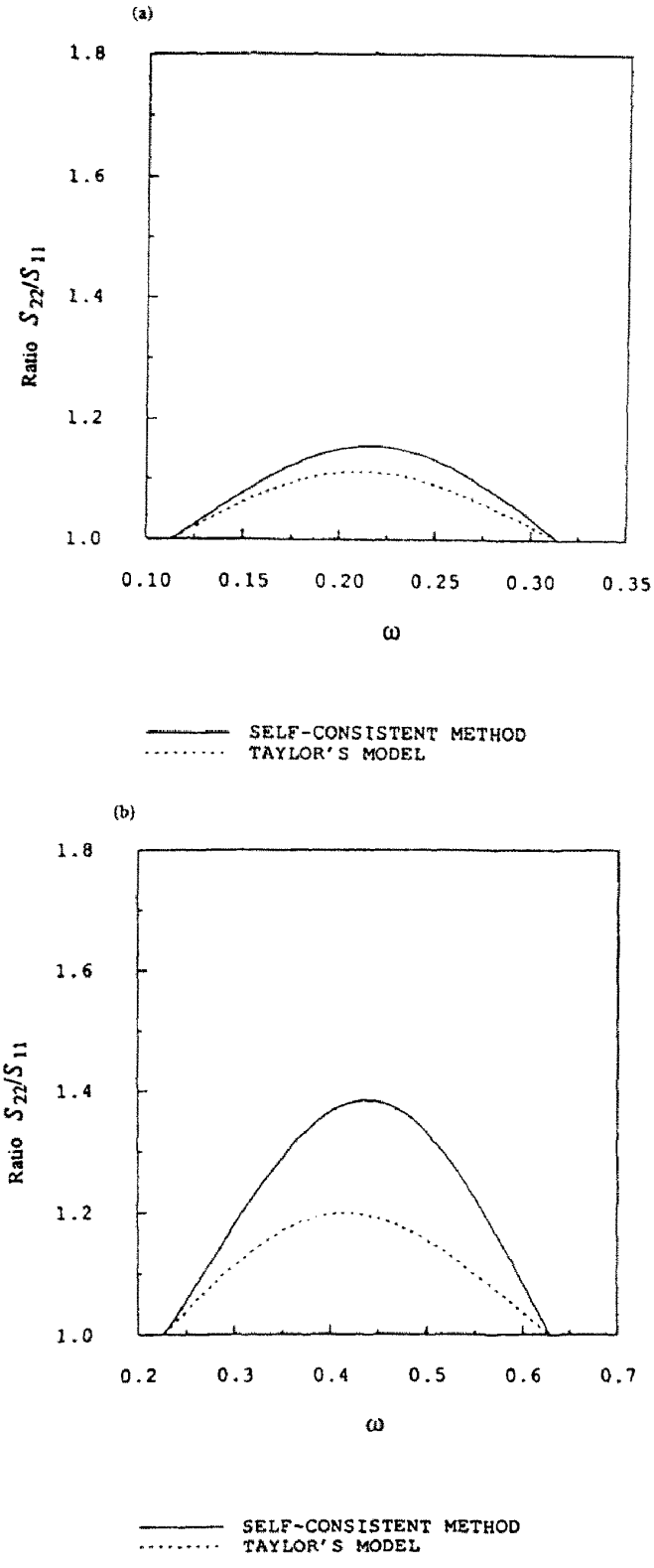

Fig. 7. S_{22}/S_{11} ratio vs the microcrack concentration parameter ω for $\omega_0 = 0.1131$ (a) and 0.2262 (b), respectively.

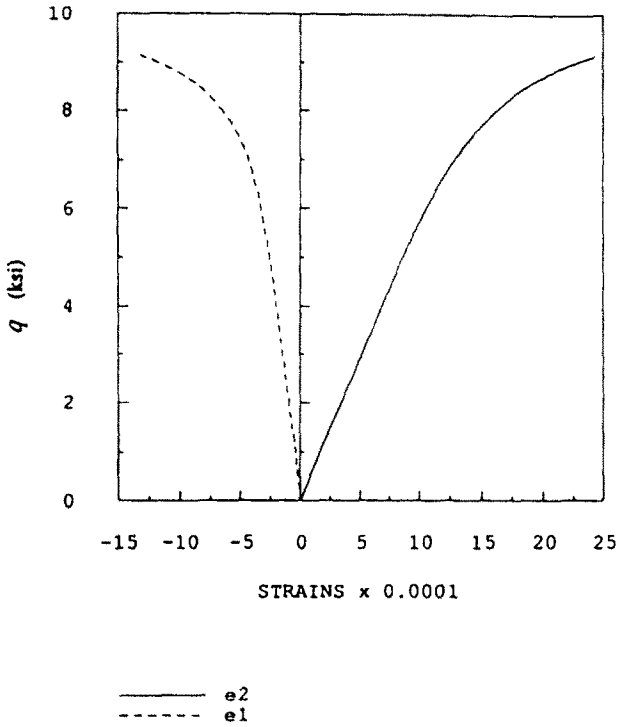

Fig. 8. The axial stress q vs the axial ($\bar{e}_2$) and lateral ($\bar{e}_1$) strains for the uniaxial compression test.

The macroscopic axial stress vs the axial (2-direction) and lateral (1-direction) strain curves are plotted in Fig. 8 for the plane strain *uniaxial compression* test. The mode II microcrack propagation and kinking threshold stresses are found to be $q_0^{II} = 1.27$ ksi (8.76 MPa) and $q_{kink} = 1.48$ ksi (10.21 MPa). Figure 9 depicts the "*active* microcrack area-concentration" parameter $\langle \omega^a \rangle$ (defined as $N\pi\langle a^2\rangle/A$) vs the axial load q. It is emphasized that "no-slip" microcracks are *excluded* from $\langle \omega^a \rangle$ since they do not contribute to either strain or secant compliance. Moreover, no-slip and sliding angle fans are *fixed* throughout

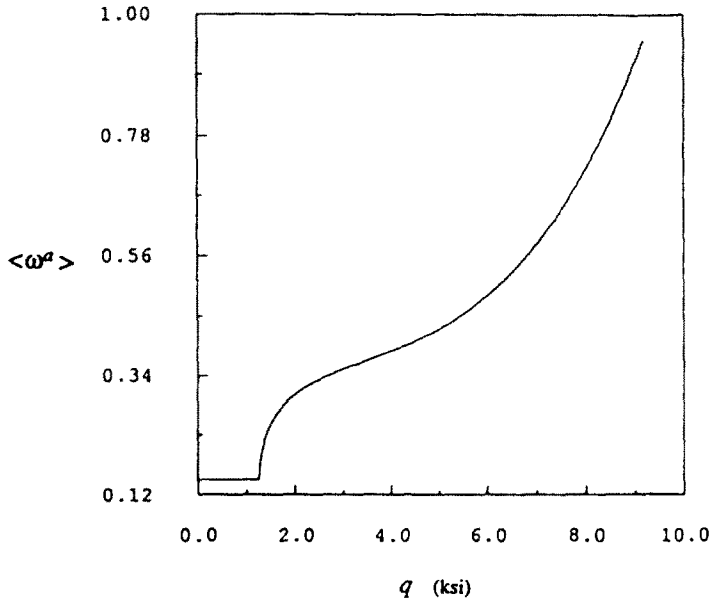

Fig. 9. The "active microcrack area-concentration" parameter $\langle \omega^a \rangle$ vs the axial stress q for the uniaxial compression test.

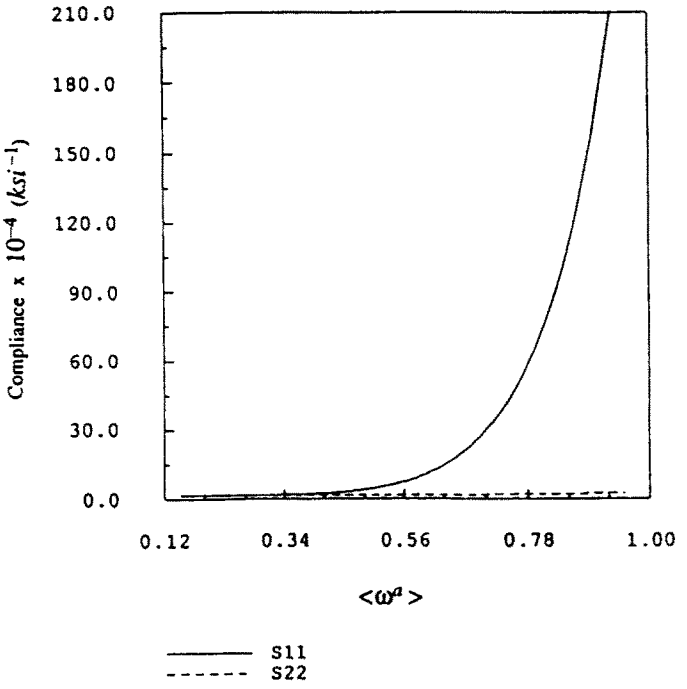

Fig. 10. $\bar{S}_{11}$ and $\bar{S}_{22}$ vs $\langle \omega^a \rangle$ for the uniaxial compression test.

the loading process. That is, $\theta_{c1} = \tan^{-1}\mu$ and $\theta_{c2} = \pi/2$. As a consequence, $\langle \omega^a \rangle$ is *fixed* before mode II microcrack propagation occurs. Figure 10 displays $\bar{S}_{11}$ and $\bar{S}_{22}$ vs $\langle \omega^a \rangle$. It is observed that the lateral compliance component $\bar{S}_{11}$ is much larger than the axial compliance component $\bar{S}_{22}$ because of the formation of many kinked microcracks. $\bar{S}_{12}$ and $\bar{S}_{21}$ vs $\langle \omega^a \rangle$ are given in Fig. 11. Notice that $\bar{S}_{21}$ is larger than $\bar{S}_{12}$ due to sliding microcrack displacements. Furthermore, Fig. 12 exhibits the shear compliance component $\bar{S}_{33}$ vs $\langle \omega^a \rangle$.

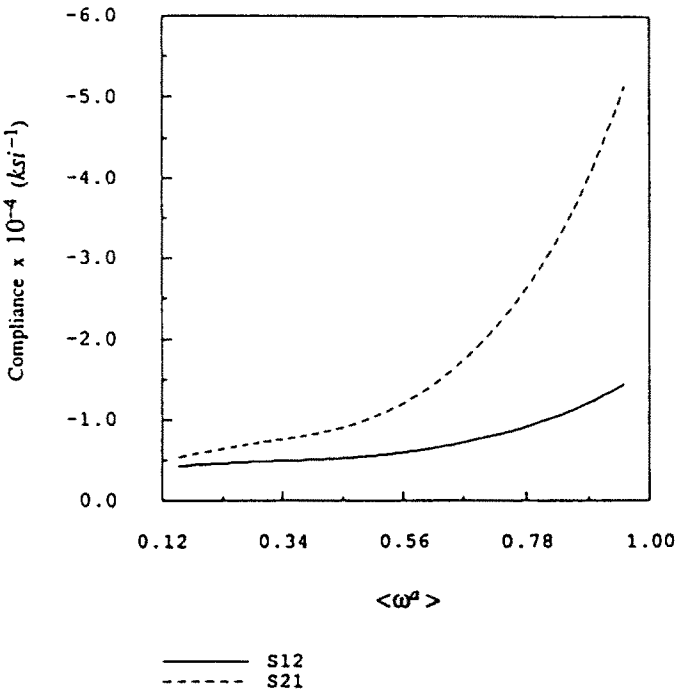

Fig. 11. $\bar{S}_{12}$ and $\bar{S}_{21}$ vs $\langle \omega^a \rangle$ for the uniaxial compression test.

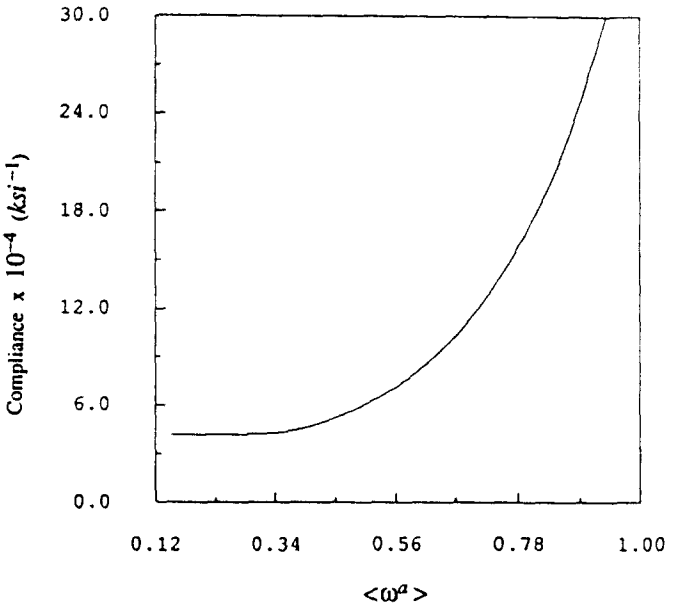

For the biaxial tension/compression test, the response is initially *isotropic* at $q = 0$ and $q^* = 0.1$ ksi (0.69 MPa, a small lateral tension) because all microcracks are initially open and of uniform size. Later, as q increases, some microcracks become closed and even become stuck (no-slip). Thus, $\bar{S}$ and $\langle\omega^a\rangle$ slightly *decrease* before mode II microcrack propagation starts. From numerical computation, the mode II microcrack propagation threshold stress is found to be $q_0^{II} = 0.95$ ksi (6.56 MPa), the microcrack kinking threshold stress $q_{kink} = 1.17$ ksi (8.07 MPa), and the mixed mode threshold stress $q_0^m = 1.28$ ksi (8.83 MPa). This implies that mode II microcrack growth in *closed* domain occurs well before

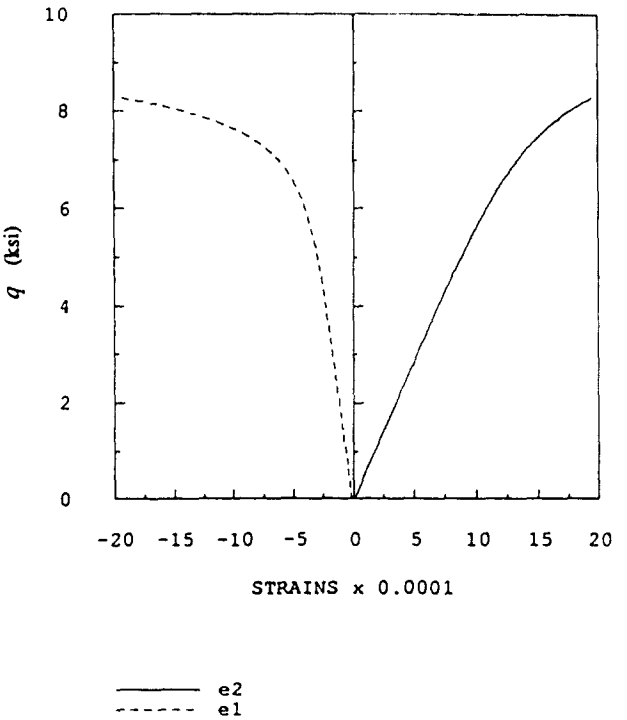

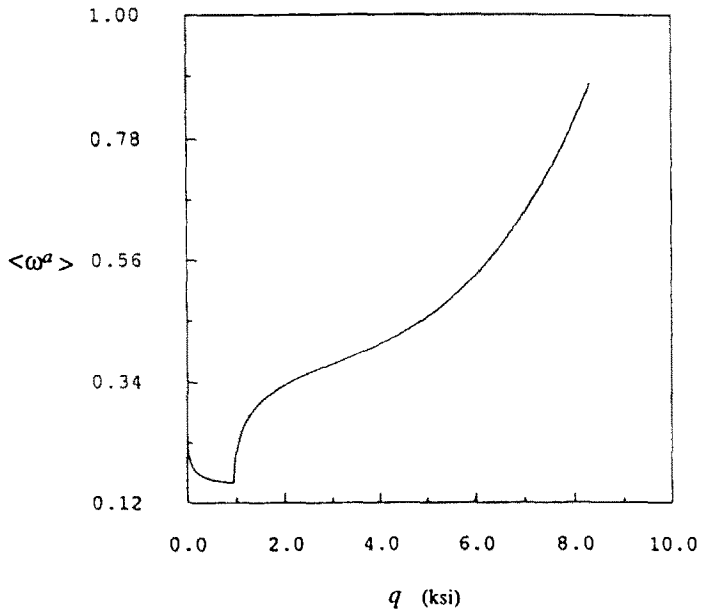

Fig. 14. The "active microcrack area-concentration" parameter $\langle \omega^a \rangle$ vs the axial stress q for the biaxial tension/compression test.

mixed mode microcrack growth takes place in *open* domain. Eventually, it is numerically observed that $\theta_{n_2}^{\mathrm{II}} = \theta_{\mathrm{b}} = \theta_{\mathrm{nl}}^{\mathrm{III}}$. The macroscopic axial stress vs the axial and lateral strain curves are plotted in Fig. 13. Figure 14 shows $\langle \omega^a \rangle$ vs the axial load q. Figure 15 displays $\bar{S}_{11}$ and $\bar{S}_{22}$ vs $\langle \omega^a \rangle$. Again, $\bar{S}_{11}$ is much larger than $\bar{S}_{22}$ because of kinked microcracks. $\bar{S}_{12}$ and $\bar{S}_{21}$ vs $\langle \omega^a \rangle$ are shown in Fig. 16. Figure 17 gives the shear compliance component $\bar{S}_{44}$ vs $\langle \omega^a \rangle$. Note that $\bar{S}_{11}$, $\bar{S}_{22}$ and $\bar{S}_{44}$ slightly decrease at the beginning due to the increase of "no-slip" microcrack domain.

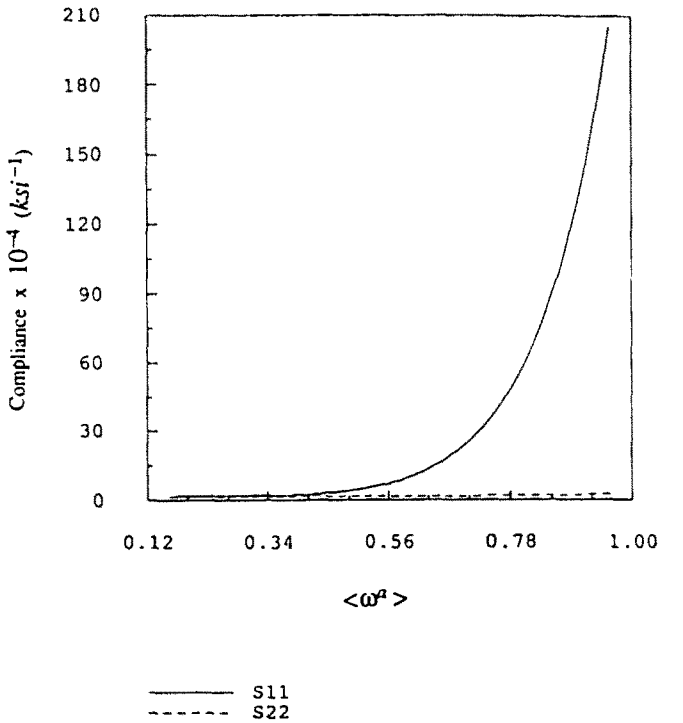

Fig. 15. $\bar{S}_{11}$ and $\bar{S}_{22}$ vs $\langle \omega^a \rangle$ for the biaxial tension/compression test.

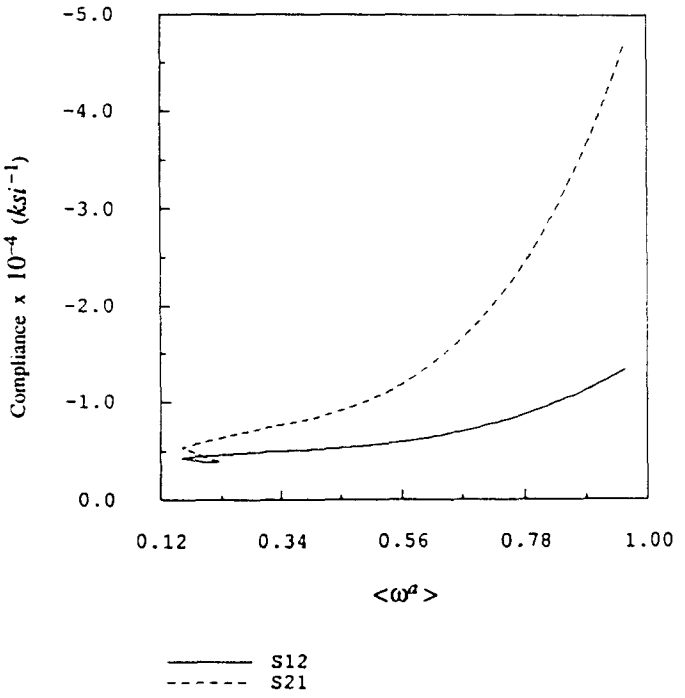

Fig. 16. $\bar{S}_{12}$ and $\bar{S}_{21}$ vs $\langle \omega^a \rangle$ for the biaxial tension/compression test.

By comparing Fig. 8 with Fig. 13, it is seen that microcrack propagation and kinking threshold stresses q_0^{II} and q_{kink} as well as the peak stress significantly decrease in the presence of a small lateral tension q^*. In addition, the lateral strain of the biaxial tension/compression test is higher than that of the uniaxial compression test.

5. CLOSURE

Following the framework proposed by Krajcinovic and Fanella (1986), the proposed micromechanical brittle damage models do not require the use of additional fitted "material

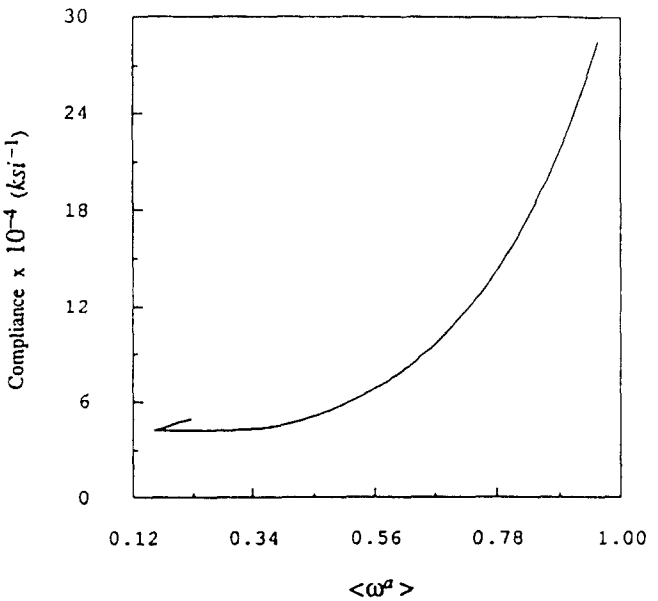

Fig. 17. $\bar{S}_{11}$ vs $\langle \omega^a \rangle$ for the biaxial tension/compression test.

parameters" other than well-defined elastic constants and fracture toughness of constituent phases. Thermodynamic basis, effective averaged field equations, microcrack opening displacements and damage-induced inelastic compliance are given within the context of two-dimensional self-consistent method. It is emphasized that secant compliances are generally non-symmetric.

Fracture mechanics stability criteria together with microstructural geometry are employed to characterize microcrack evolutions under mode I, mode II and mixed mode. Simple and efficient computational algorithms are presented. In addition, three detailed numerical simulations are given. Finally, it is emphasized that loading/unloading stress paths and microcrack opening/closing status changes are easily accommodated with the context of the proposed damage models.

Acknowledgements—This work was sponsored by the Air Force Office of Scientific Research under Grant No. AFOSR-88-0324, together with the Defense Nuclear Agency. The author gratefully acknowledges this support and the interest of Dr Spencer T. Wu, Dr Paul Senseny and Dr Kent L. Goering. The author is also indebted to Dr X. Lee for his numerical calculations and valuable contributions to this work.

REFERENCES

Ashby, M. F. (1979). Micromechanisms of fracture in static and cyclic failure. In *Fracture Mechanics, Current Status, Future Prospects* (Edited by R. A. Smith), Vol. 1. Pergamon, Oxford.

Budiansky, B. and O'Connell, R. J. (1976). Elastic moduli of a cracked solid. *Int. J. Solids Structures* **12**, 81–97.

Chudnovsky, A., Dolgopolsky, A. and Kachanov, M. (1987a). Elastic interaction of a crack with a microcrack array—I: Formulation of the problem and general form of the solution. *Int. J. Solids Structures* **23**(1), 1–10.

Chudnovsky, A., Dolgopolsky, A. and Kachanov, M. (1987b). Elastic interaction of a crack with a microcrack array—II: Elastic solution for two crack configurations (piece-wise constant and linear approximations). *Int. J. Solids Structures* **23**(1), 11–21.

Fanella, D. and Krajcinovic, D. (1988). A micromechanical model for concrete in compression. *Engng Fracture Mech.* **29**(1), 49–66.

Hill, R. (1965). A self-consistent mechanics of composite materials. *J. Mech. Phys. Solids* **13**, 213–222.

Hoenig, A. (1978). The behavior of a flat elliptical crack in an anisotropic elastic body. *Int. J. Solids Structures* **14**, 925–934.

Hoenig, A. (1979). Elastic moduli of a non-randomly cracked body. *Int. J. Solids Structures* **15**, 137–154.

Hoenig, A. (1982). Near-tip behavior of a crack in a plane anisotropic elastic body. *Engng Fracture Mech.* **16**(3), 393–403.

Horii, H. and Nemat-Nasser, S. (1983). Overall moduli of solids with microcracks: load induced anisotropy. *J. Mech. Phys. Solids* **31**(2), 155–171.

Horii, H. and Nemat-Nasser, S. (1985a). Elastic fields of interacting inhomogeneities. *Int. J. Solids Structures* **21**(7), 731–745.

Horii, H. and Nemat-Nasser, S. (1985b). Compression induced microcrack growth in brittle solids: axial splitting and shear failure. *J. Geophys. Res.* **90**, 3105–3125.

Horii, H. and Nemat-Nasser, S. (1986). Brittle failure in compression: splitting, faulting and brittle-ductile transition. *Phil. Trans. R. Soc.* **319**, 337–374.

Ju, J. W. (1989). On energy-based coupled elastoplastic damage theories: Constitutive modeling and computational aspects. *Int. J. Solids Structures* **25**(7), 803–833.

Kachanov, L. M. (1958). Time of the rupture process under creep conditions. *IVZ Akad Nauk, S.S.R.* Otd Tech Nauk **8**, 26–31.

Kachanov, M. (1980). Continuum model of medium with cracks. *J. Engng Mech. Div., ASCE* **106**, (EM5), 1039–1051.

Kachanov, M. (1987). Elastic solids with many cracks: A simple method of analysis. *Int. J. Solids Structures* **23**(1), 23–43.

Kanninen, M. F. and Popelar, C. H. (1985). *Advanced Fracture Mechanics*. Oxford University Press, New York and Clarendon Press, Oxford.

Krajcinovic, D. (1984). Continuum damage mechanics. *Appl. Mech. Rev.* **37**(1–6), 397–402.

Krajcinovic, D. (1985). Constitutive theories for solids with defective microstructure. In *Damage Mechanics and Continuum Modeling* (Edited by N. Stubbs and D. Krajcinovic), pp. 39–56. ASCE.

Krajcinovic, D. (1986). Update to continuum damage mechanics. In *Appl. Mech. Update*, pp. 403–406.

Krajcinovic, D. and Fanella, D. (1986). A micromechanical damage model for concrete. *Engng Fracture Mech.* **25**(5–6), 585–596.

Krajcinovic, D. and Sumarac, D. (1989). A mesomechanical model for brittle deformation processes: Part I. *J. Appl. Mech.* **56**(3), 51–56.

Lekhnitskii, S. G. (1950). *Theory of Elasticity of an Anisotropic Elastic Body*. The Government Publishing House for Technical Theoretical Works, Moscow and Leningrad, 1950; Holden-Day, San Francisco, 1963.

Mura, T. (1982). *Micromechanics of Defects in Solids*. Nijhoff, The Hague.

Nemat-Nasser, S. and Horii, H. (1982). Compression-induced nonplanar crack extension with application to splitting, exfoliation, and rock-burst. *J. Geophys. Res.* **87**, 6805–6821.

Ortiz, M. (1985). A constitutive theory for the inelastic behavior of concrete. *Mech. Mater.* **4**, 67–93.

Rice, J. R. (1975). Continuum mechanics and thermodynamics of plasticity in relation to microscale deformation mechanisms. In *Constitutive Equations in Plasticity* (Edited by A. Argon). MIT Press, Cambridge, MA.

Sih, G. C., Paris, P. C. and Irwin, G. R. (1965). On cracks in rectilinearly anisotropic bodies. *Int. J. Fracture Mech.* **1**(3), 189–203.

Simo, J. C. and Ju, J. W. (1987). Stress and strain based continuum damage models. Part I: Formulation. *Int. J. Solids Structures* **23**(7), 821–840.

Sneddon, I. N. and Lowengrub, M. (1969). *Crack Problems in the Classical Theory of Elasticity*. Wiley, New York.

Sumarac, D. and Krajcinovic, D. (1987). A self-consistent model for microcrack-weakened solids. *Mech. Mater.* **6**, 39–52.

Sumarac, D. and Krajcinovic, D. (1989). A mesomechanical model for brittle deformation processes: Part II. *J. Appl. Mech.* **56**(3), 57–62.

Vakulenko, A. A. and Kachanov, M. L. (1971). Continuum theory of medium with cracks. *Mekh. Tverdogo Tela* **4**, 159–166.

Willis, J. R. (1968). The stress field around an elliptical crack in an anisotropic elastic medium. *Int. J. Engng Sci.* **6**, 253–263.

Wu, C. H. (1985). Tension-compression test of a concrete specimen via a structure damage theory. In *Damage Mechanics and Continuum Modeling* (Edited by N. Stubbs and D. Krajcinovic), pp. 1–12. ASCE, New York.

Zaitsev, Y. (1982). *Deformation and Strength Models for Concrete Based on Fracture Mechanics*. Stroiizdat, Moscow.

Zaitsev, Y. (1983). Crack propagation in a composite material. In *Fracture Mechanics of Concrete* (Edited by F. H. Wittmann), pp. 251–299. Elsevier, Amsterdam.